Journal of Atmospheric and Solar–Terrestrial Physics 280 (2026) 106760

Contents lists available at ScienceDirect

Journal of Atmospheric and Solar–Terrestrial Physics

journal homepage: www.elsevier.com/locate/jastp

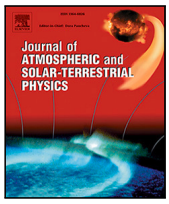

Research paper

Decadal variability in mid-atmosphere temperature derived from continuous lidar observations

Pedro Da Costa Louro [a,*], Philippe Keckhut [a], Alain Hauchecorne [a,h], Robin Wing [b], Gerd Baumgarten [b], Michael Gerding [b], Thierry Leblanc [c], Bernd Kaifler [d], Natalie Kaifler [d], Wolfgang Steinbrecht [e], Ali Jalali [f], Robert J. Sica [g]

[a] *Laboratoire Atmosphères, Observations Spatiales (LATMOS), Institut Pierre-Simon Laplace, Université Versailles-Saint Quentin, Université Paris-Saclay, 78280 Guyancourt, France*
[b] *Leibniz-Institut für Atmosphärenphysik an der Universität Rostock, Kühlungsborn, Germany*
[c] *Jet Propulsion Laboratory, California Institute of Technology, Wrightwood, CA 92397, USA*
[d] *Deutsches Zentrum für Luft- und Raumfahrt, Institut für Physik der Atmosphäre, Oberpfaffenhofen, Germany*
[e] *Deutscher Wetterdienst, Meteorologisches Observatorium, 82383 Hohenpeissenberg, Germany*
[f] *Newfoundland and Labrador Weather Office, Meteorological Service of Canada, Environment and Climate Change Canada, Gander, Newfoundland and Labrador, Canada*
[g] *Department of Physics and Astronomy, The University of Western Ontario, London, N6A 3K7, Canada*
[h] *Gordien Strato, 11 Boulevard d'Alembert, 78280 Guyancourt, France*

ARTICLE INFO

Dataset link: http://www.ndacc.org, https://www.aeris-data.fr/, https://cds.climate.copernicus.eu/, https://lasp.colorado.edu/lisird/data/penticton_radio_flux, https://www.atmohub.kit.edu/english/807.php, https://ccmc.gsfc.nasa.gov/models/NRLMSIS~2.0/, https://dx.doi.org/10.60897/x48r-e929, https://doi.org/10.5281/zenodo.17241353, 10.22000/fncjgk3afh2qt1dw

Keywords:
Atmosphere
Sun–earth interactions
Lidars
Climatology
Global warming

ABSTRACT

Nine Rayleigh scattering-based lidars, some of which are affiliated with the Network for the Detection of Atmospheric Composition Change (NDACC) and the Atmospheric Remote Sensing in Stratosphere and mesosphere (ARISE) for monitoring stratospheric ozone, have been routinely observing temperature profile variations in the middle atmosphere for many years with excellent vertical resolution (around one kilometer). These observatories are located at various points around the globe from north to south: ALOMAR in Norway, Kühlungsborn in Mecklenburg-Western Pomerania Germany, Hohenpeissenberg in Bavaria Germany, Haute-Provence in southern France, Purple Crow in the Canadian London Ontario, Table Mountain in California, Mauna Loa in Hawaii, Maido on Reunion Island, Coral in Tierra del Fuego Argentina . These unique datasets have made it possible to update the climatology and seasonal variations of middle atmosphere temperatures between 30 and 80 km at several latitudes with significantly long databases that could be compared with numerical models. The behavior is similar at all sites, with a marked annual variation in the stratosphere of up to 6K, little variation around the stratopause (≈ 2K) and a continuously increasing seasonal variation in the mesosphere of up to 16 K for some sites. These seasonal cycles are halved in tropical sites. The QBO (Quasi-Biennial Oscillation) is clearly visible in the temperature series and causes variations that can exceed 1 K. The temporal extent of the series, spanning several 11-year solar cycles, made it possible to extract variations associated with changes in solar activity on the vertical temperature profile, showing signatures of up to 4 K. In summer at mid and low latitudes, the signature is weak and around 1 K, in line with the expected photochemical effects. In winter, the response at mid-latitudes confirms previous observations of a negative effect. At higher latitudes, even larger signatures are observed, confirming the effect of feedback in the atmospheric response. This analysis also allowed us to update the quantification of decadal trends in the middle atmosphere, which show differences depending on latitude. These fluctuations become significant when the series are longer than one solar cycle. Observations at mid and low latitudes confirm the significant detection of a cooling ranging from about 1 K/decade in the upper stratosphere and increasing in the mesosphere to several K/decade. At mid latitudes, the three sites show good agreement, but in tropical/subtropical regions, greater variability is observed. In particular, in the mesosphere, observations obtained over Reunion Island in the tropical region in the southern hemisphere show cooling of up to 5 K/decade in the mesosphere, significantly greater than at other sites. Polar lidar data show that in these regions the trend is towards warming, with values remaining around 2K/decade, mainly in the mesosphere however the variability is large and the sampling larger in winter.

* Corresponding author.
E-mail address: pedro.da-costa@latmos.ipsl.fr (P. Da Costa Louro).

https://doi.org/10.1016/j.jastp.2026.106760
Received 30 October 2025; Received in revised form 29 January 2026; Accepted 7 February 2026
Available online 17 February 2026

1. Introduction

The evolution of the temperature of the Middle Atmosphere (MA) that range from the tropopause (≈15 km) to the mesopause (≈80 km) is an interesting indicator to monitor regarding climate change. The MA, being influenced by both the troposphere (0–15 km) and the thermosphere (>100 km), serves as a tracer that allows tracking various external natural phenomena (solar activity, volcanic injections), internal variability (Quasi-Biennial Oscillation, QBO), and anthropogenic effects that increase the amount of greenhouse gases and reduce the amount of stratospheric ozone due to ozone-depleting substances (ODS) ((WMO) et al., 2023).

The determination of robust climatological trends in the middle atmosphere often relies on the analysis of time series from a single instrument, an approach that avoids systematic biases and discontinuities associated with the cross-referencing of heterogeneous datasets. However, these single-instrument series rarely exceed a decade, which severely limits our ability to isolate and characterize the climate response to low-frequency natural forcings, such as the 11-year solar cycle or persistent disturbances induced by major volcanic eruptions. In the absence of such long series, it becomes difficult to distinguish true climate variability from potential instrumental artefacts or incomplete modeling of other periodic phenomena, such as atmospheric tides (Keckhut et al., 2011). The increase in the number of instruments dedicated to observing the stratosphere prompted the publication of a comprehensive study (Steiner et al., 2020). This study aggregates all the data collected between 1979 and 2018 using various methods (radiosondes, SSU, SSU merged, MSU/AMSU, radio occultation and lidars). The integrated analysis of these datasets indicates an average cooling of the stratosphere of between 0.25 and 0.75 K per decades. Unlike the stratosphere, climatological studies of the mesosphere are hampered by a lack of systematic long-term observations. The complexity of observing this layer explains the scarcity of continuous instrumental data series. Existing studies, which generally favor the use of a single type of instrument (MLS and SABER satellites, ground-based lidars, OSIRIS spectrometer) to ensure data homogeneity and avoid inter-instrument artefacts, rarely cover more than a decade. In the absence of an integrative synthesis comparable to that available for the stratosphere, the cooling trend must be deduced from the convergent analysis of several individual studies (Dube et al., 2024; Hauchecorne et al., 1991; Steinbrecht et al., 2025; Zhao et al., 2021; Kishore et al., 2014; Beig et al., 2003; Beig, 2011). These studies report even more pronounced mesospheric cooling than in the stratosphere, with estimated rates, depending on the instrument and geographical region, ranging from 0.5 to 2 K per decade. Previous studies indicate that solar flux forcing on the temperature of the middle atmosphere induces variations of around ±2 K per 100 solar flux units (sfu), with an amplitude that tends to increase with altitude. The quasi-biennial oscillation (QBO) mainly affects the stratosphere, where it generates anomalies of up to ±1.5 K for a 10 m s^{-1} variation in the zonal wind; its influence then decreases significantly with altitude. However, these natural signals remain much smaller than the dominant seasonal variability, driven by annual and semi-annual cycles, whose amplitude can exceed 20 K in the upper mesosphere.

The ERA5 and MERRA-2 atmospheric reanalysis models, widely used for studying the middle atmosphere, show trends whose degree of agreement depends heavily on the pressure level considered. At 100 hPa, the two datasets are broadly consistent, showing a heterogeneous geographical structure with local trends varying between −0.5 and 0.5 K per decade. This relative agreement continues at 50 hPa, although a notable divergence already appears above the South Pole, where ERA5 detects a slight warming of approximately 0.3 K/decade that is absent in MERRA-2, which instead observes a continuous cooling. The divergence becomes much more pronounced at 10 hPa. At this level, MERRA-2 simulates a pronounced and almost global cooling of around −1.2 to −1.5 K/decade, while ERA5 indicates only a much more moderate cooling of around −0.3 K/decade. At 1 hPa, the signals become completely opposite. MERRA-2 suggests near-global warming of up to 1.5 K/decade, while ERA5 shows cooling of the same maximum magnitude, −1.5 K/decade. A notable exception to this opposition is the polar region, for which the two reanalyses agree, at almost all levels, on a strong warming of around 1.5 K/decade. This polar concordance disappears at 1 hPa in ERA5, which no longer shows a uniform signal there (Kozubek et al., 2021).

To understand stratospheric processes and their link with ozone, continuous monitoring of temperature became essential however, the number of future measurements in the stratosphere will be reduced in the coming years, so ground-based data will be essential to ensure temporal continuity (Salawitch et al., 2025). Temperature strongly controls the balance of ozone production, while ozone itself influences the radiative budget through solar absorption. For this reason, temperature measurements were implemented alongside ozone monitoring within the Network for the Detection of Stratospheric Changes (Kurylo and Solomon, 1990; Organization et al., 2018). Rayleigh lidars, capable of providing high-vertical-resolution temperature profiles between 30 and 80 km (Hauchecorne and Chanin, 1980), were deployed at sites from the poles to the equator. One of the first instruments was installed at the Haute-Provence Observatory, where more than 40 years of continuous records have been collected, averaging around 100 nighttime temperature profiles per year.

The challenge in estimating interannual changes that could be associated with anthropogenic causes is confronted with the need for long series to reduce uncertainties and avoid interference between solar activity, QBO, and anthropogenic variations. It is also necessary to consider that trends are estimated in a changing environment (Kerzenmacher et al., 2006). For example, the emission of ozone-depleting substances has been completely halted as they have been banned since 1997, although it will take about five decades for chlorinated species to be significantly reduced in the atmosphere. However, the increase in greenhouse gases, which continues to rise exponentially, will keep modifying our atmosphere, and we can expect retroactive effects, particularly on atmospheric dynamics, leading to variable trends over time and across different regions.

This study focuses on estimating trends from several lidars that have operated for a minimum duration exceeding a solar cycle. Some datasets that had already been studied were revised, and others have reached durations allowing, for the first time, an investigation. This study is based on the standard method of multi-parameter linear regression. In addition to a linear response, the main proxies considered are seasonal cycles, variations in solar activity, and the Quasi-Biennial Oscillation (QBO). This method also provides updated information on average climatology and the response of the middle atmosphere to these forcings.

After describing the datasets and proxies used in Section 2, Section 3 outlines the methodology and analysis of seasonal variations. Section 4 presents the responses to interannual variations. Section 5 examines the residuals, and finally, Section 6 discusses the results and concludes with these new estimates.

2. Description of the datasets

2.1. The Rayleigh lidar

The data used in this study were obtained from molecular scattering lidars, also known as Rayleigh lidars. The method is based on the backscattering of a pulsed laser beam by atmospheric molecules. By studying the echo over time, the vertical profile of atmospheric density is obtained in relative values. Based on hydrostatic equilibrium and the ideal gas law, the absolute temperature profile is deduced (Hauchecorne and Chanin, 1980; Chanin and Hauchecorne, 1984; Sica and Haefele, 2015).

This method allows obtaining a temperature profile in the range of 30 to about 80 km with unparalleled resolution. Lidars often have an electronic resolution between 10 to 100 m. The main uncertainty corresponds to the statistical error of photon counting, which is simple to evaluate from the number of photons collected as it is well modeled and mainly depends on the laser power and the size of the collector (often a telescope). For precision and atmospheric monitoring purposes, the initial resolution is often degraded to around 1 km and around 1 h of integration, which remains excellent compared to other existing observations in the mesosphere for estimating trends (Beig et al., 2003).

Due to the decrease in atmospheric density with altitude, precision decreases. Three altitude ranges can be identified with the following uncertainties in averaged (Hauchecorne et al., 1991):

- From 30 to 70 km: <0.3% in density / <1 K in temperature
- From 80 km: 1% in density / 3 K in temperature
- From 90 km: 3% in density / 10 K in temperature

The second uncertainty is due to noise sources induced by optical and electronic effects, which are more difficult to evaluate. Data inversion requires an initialization of the density profile, introducing an uncertainty that quickly becomes negligible as altitude decreases.

The first instruments to operate regularly did so within the framework of the Network for the Detection of Atmospheric Composition Change (NDACC). This international organization primarily aims to study ozone series and parameters associated with its variability, including temperature. These systematic observations have been conducted from the ground through a network of stations worldwide. In addition to the interannual monitoring of stratospheric ozone and associated parameters, the objectives focus on the long term to validate sensors onboard satellites. The network was also originally created to ensure the validation of the UARS satellite (Fishbein et al., 1996; Hervig et al., 1996; Gille et al., 1996).

The network implements different techniques to validate these instruments, such as using artificial signals (Leblanc et al., 1998a) and campaigns with a reference instrument. Regarding the Haute Provence Observatory data, two additional lidars at the same latitude and only 550 km apart measured the MA temperature simultaneously for 65 nights. The geographical separation being small, the expected difference between the average temperature profiles of the two lidars is close to 0 K (Keckhut et al., 1993). More recently, on the same site, the ozone lidar provided a temperature profile compared to that given by the historical lidar (Wing et al., 2018). Thanks to this, an error of less than 2 K between 30 and 80 km was estimated, and comparisons with radiosondes at 30 km confirmed this value. Inter-comparisons were also performed from site to site with a mobile lidar deployed by NASA and in the case of the LAVANDE experiment (Keckhut et al., 2004; Wing et al., 2020). Recently, other lidars have been developed to complement those of the NDACC network and integrated into a network focusing on the dynamics of the upper atmosphere within the European infrastructure ARISE (Blanc et al., 2017). As part of this project, a particular effort was made to extend the observations of dynamic parameters using several techniques such as infrasound, microwaves, and lidars. Wind lidars were developed, and other Rayleigh lidars operated to provide additional observations.

2.2. Lidars used

For this climatological study, we selected 9 lidars from the NDACC and ARISE networks that have been producing temperature data series for several decades.

The Haute-Provence Observatory (OHP) located in France at 43.94°N, 5.71°E, at an altitude of 650 m, is the oldest active lidar station for temperature measurement. It produces about 100 temperature profiles per year since late 1978 with almost no interruption. The NASA mobile lidar (McGee et al., 1991) has been intercompared three times with this lidar (Singh et al., 1996; Braathen et al., 2004; Wing et al., 2020). This series has already been used to estimate interannual variability (Tufel et al., 2025) and trends (Hauchecorne et al., 1991; Keckhut et al., 1995; Steinbrecht et al., 2009; Angot et al., 2012), but it has not been updated for over 10 years.

Hohenpeissenberg (HOH), located in southern Germany at 47.80°N, 11.02°E, at an altitude of 980 m, has been producing temperature profiles since 1987 without interruption, with an average of 90 profiles per year. The instrument was initially designed to measure the ozone profile using the DIAL method, and then the off-axis channel of the instrument was used to deduce the temperature. Trends have also been obtained from this instrument along with other sites (Steinbrecht et al., 2009; Wing et al., 2021).

Table Mountain Facility (TMF), located in California at 34.4°N, 117.7°W, at an altitude of 2300 m, produces about 110 temperature profiles per year since 1989 with a measurement interruption between 2013 and 2017 (Leblanc et al., 1998b).

Mauna Loa (MLO), located in Hawaii at 19° 54′N, 155.58° W, at an altitude of 3397 m, produces about 163 temperature profiles per year since 1999 with a measurement interruption between 2022 and 2024. This station, like the previous one, is operated by NASA (Leblanc et al., 1998b). Trends were evaluated for these two sites in 2011 (Li et al., 2011).

Réunion Island (RUN) has two successive measurement sites: one in St. Denis at 20.9°S, 55.5°E, at an altitude of 85 m, which produced temperature profiles from 1994 to 2009, and another site at a higher altitude in Maido at 21.1°S, 55.4°E, at an altitude of 2155 m, which has been producing temperature profiles since 2013. On average, these two sites have produced 54 profiles per year (Baray et al., 2013).

Kühlungsborn (KUH), located in northern Germany at 54.1°N, 11.7° E, has been producing temperature profiles since 2012 with about 66 profiles per year without interruption (Gerding et al., 2016).

CORAL (COR), the newest lidar in this study, is located in Tierra del Fuego, Argentina, at 53.7°S, 67.7°E. It has been producing data since 2017 with an average of 137 profiles per year (Kaifler and Kaifler, 2021).

ALOMAR (ALO), located in northern Norway at 69.3°N, 16°E, observes the middle atmosphere throughout the year since 2003 with a little more than 40 observations per year (Von Zahn et al., 2000; Fiedler and Baumgarten, 2024).

Purple Crow (PCL), located in the Canadian Great Lakes region at 42.5°N, 81.2°W, is unfortunately the only lidar that is no longer active in this study. Its observations lasted 20 years from 1994 to 2013, with an average of 25 observations per year (Sica et al., 1995; Jalali et al., 2018).

To maintain data uniformity, all profiles are interpolated with a 1 km step from 30 to 70/80 km, except for the KUH lidar, which starts at 40 km. The temperature profiles studied in this study are the averages of the profiles obtained over 2 to 4 h of measurements centered on midnight local time.

Fig. 1 shows the geographical location of each lidar as well as the start and end years of measurements for our study.

2.3. Description of the ERA5 and MSIS 2.0 models

MSIS is a climate model developed by the Naval Research Laboratory (NRL) that has recently been updated to version 2.0 (Emmert et al., 2021). It describes the average behavior of temperature, the density of numerous chemical species, and mass density through an analytical formulation. It integrates seasonal variations, fluctuations based on altitude, latitude, and longitude. The main input data are the date within the year, geographic coordinates, and the altitude range, allowing for the retrieval of a vertical profile.

ERA5, on the other hand, is a reanalysis produced by the ECMWF (European Centre for Medium-Range Weather Forecasts). It is based on

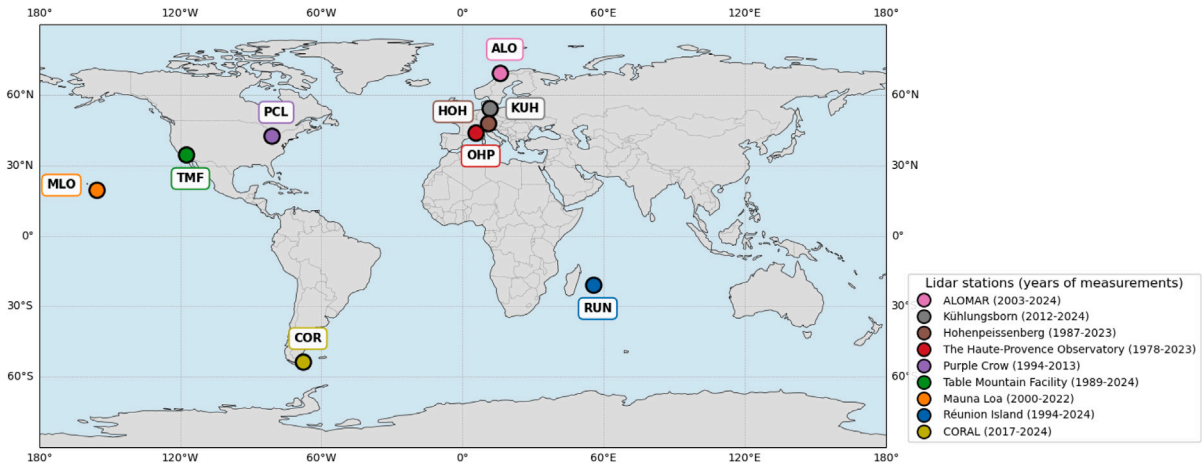

Fig. 1. World map showing the geographical location of each lidar. In the legend, you can find the start year and end year of measurements for each lidar used in the study.

meteorological fields provided by a unique weather model and continuously guided by diverse and global observations covering the last seven decades. This analysis provides estimates of numerous atmospheric climate variables for each day. The data used are resolved on 137 levels ranging from the surface to about 80 km (Hersbach et al., 2020).

The data assimilated into the ERA5 model for temperature include:

- Between 1979 and 2005, the Stratospheric Sounding Unit (SSU) onboard TIROS-N, NOAA-6 to -9, -11, and -14, which provides temperature information between 30 and 50 km. There were 1 to 2 satellites available throughout this period.
- The multispectral IR sounders (HIRS from 1979 and VTPR from 1972 to 1978) have channels that provide temperature information in the lower to middle stratosphere, from 26 to 43 km.
- Starting in 1998, the Advanced Sounding Unit (AMSU-A) instrument, onboard NOAA-15 to -19, Metop-A/-B/-C, continues to provide temperature information between 30 and 50 km. The increasing number of available instruments raises the number of assimilations to 5 by 2005.
- GNSS-Radio Occultation (RO) data providing temperature information up to 50 km, starting from 2002 (CHAMP), but in greater numbers after 2006 (COSMIC). By 2019, nearly 10 instruments were being assimilated into the ERA5 temperature model.

MSIS and ERA5 operate differently. MSIS covers a broader vertical domain from 0 to 1000 km, while ERA5, with its 137 levels, is limited to the mesopause with a so-called "sponge" region in its upper part in the mesosphere (Polichtchouk et al., 2022). ERA5 provides a vast amount of atmospheric information, but here only the temperature, pressure, and density profiles for this study. Previous comparisons have shown very good agreement between lidars and meteorological analyses in the stratosphere but significant differences in the mesosphere (Marlton et al., 2021; Mariaccia et al., 2022). It should be noted that no observations are assimilated into the model above 50 km.

3. Description of the analysis method

A multiple linear regression is applied to all lidar databases, altitude by altitude, to better understand temperature variations, their anthropogenic trends, and other interannual variations of natural origin. This analysis is conducted independently with a vertical resolution of 1 km. The method involves modeling variations using proxies that characterize the fluctuations of forcing over time. The least squares regression allows for the deduction of a coefficient corresponding to the atmospheric response to each of the forcings to best represent the observations. In this analysis, the responses are assumed to be linear with respect to the proxy used.

For the studied altitude range, we chose to represent seasonal cycles using sinusoidal functions. We included in the analysis a response to the Quasi-Biennial Oscillation, a response to solar activity, particularly related to the well-known 11-year cycle, and a linear response corresponding to anthropogenic activity, whether related to ozone depletion or the increase in greenhouse gases.

Volcanoes that have sent a significant amount of dust into the stratosphere, where it remains for some time (several months), have a significant climatic impact. The evolution of the stratospheric extinction coefficient is available from CREST (Climate Data Record of Stratospheric Aerosols) (Sofieva et al., 2024). However, in this analysis, we did not include a signal related to major volcanic eruptions due to the strong non-linearity of this forcing and the impossibility of simply representing it in a linear regression. Indeed, depending on the latitude of injection and the type of aerosols, the atmospheric response can be very different. This is the case, for example, for Hunga (Khaykin et al., 2022) but also for biomass fires (Peterson et al., 2018; Khaykin et al., 2020), which through pyro-convection can influence atmospheric conditions. Following our investigations into the effect of aerosols on the temperature variations of the middle atmosphere, we chose not to consider them in this study. Indeed, the responses were not significant; it appears that each eruption must be studied separately. It is evident that the particles injected into the stratosphere by Mount Pinatubo are very different from those injected by Hunga Tonga. This analysis based on lidar data will be the subject of a subsequent specific study.

3.1. Description of proxies

3.1.1. The Quasi-Biennial Oscillation (QBO)

The Quasi-Biennial Oscillation (QBO) is a climatic phenomenon characterized by alternating east and west zonal winds in the tropical stratosphere between approximately 100 and 10 hPa. This oscillation, which lasts on average 28 months, is caused by the interaction of gravity waves and Kelvin waves with the mean zonal flow. It has dynamic and global impacts, particularly on the distribution of stratospheric ozone, tropospheric circulation patterns, and sudden stratospheric warmings. Studies have also demonstrated the connection between the QBO and global stratospheric circulation, highlighting their role in atmospheric dynamics (Lindzen and Holton, 1968; Holton and Lindzen, 1972; Dunkerton, 1997; Baldwin et al., 2001)

The Karlsruhe Institute of Technology (KIT) compiles data on daily wind observations in the stratosphere since 1957. They use data from stations near the equator, as well as data from the northern hemisphere

for earlier years. Monthly mean components of the zonal wind have been calculated for different atmospheric levels. An initial dataset was created by combining observations from three radiosonde stations: Canton Island at 2.46°S 171.43°W (closed in 1967), Gan/Maldives Islands at 0.41°S 73.09°E (closed in 1975), and Singapore at 1.22°N 103.55°E, representative of the equatorial belt since all studies have shown that longitudinal differences in the QBO phase are minimal. However, uncertainties arose due to the lack of observations at the beginning of the study period. From these daily values, the monthly mean components of the zonal wind have been calculated for the 70, 50, 40, 30, 20, 15, and 10 hPa levels from 1953 to the present.

3.1.2. Solar flux at 10.7 cm

The various manifestations of solar activity are influenced by the total amount of magnetic flux that escapes from the photosphere to the chromosphere and corona, as well as its distribution over time and space. Solar activity exhibits variations over a cycle of approximately 11 years. The 10.7 cm radio signal is a measure of the integrated emission over the solar disk. This emission is almost entirely of thermal origin and is directly related to the total amount of plasma confined in the magnetic fields of active regions.

This flux is measured from the ground by the Solar Radio Monitoring Program, a service managed by the National Research Council and Natural Resources Canada with support from the Canadian Space Agency. This program uses two instruments that record the intensity of solar radio emissions at the aforementioned wavelength of 10.7 cm. Recordings are made every day except during maintenance or system testing, allowing their database to have solar flux values almost every day since 1947. This solar activity indicator is correlated with variations in solar flux and is very useful for monitoring solar activity. Indeed, measurements in the UV range are not possible from the ground and are difficult to inter-calibrate from space.

3.2. Description of linear regression

The linear regression method used in this study is described below. It is applied independently to each altitude level in the temperature time series. In order to ensure the statistical independence of the successive samples required by this method, and given that the autocorrelation of the temperature data is less than one week (Hauchecorne et al., 1991; Keckhut et al., 1995), the dataset was homogenized on a weekly basis. To do this, lidar temperature measurements and solar flux values were averaged over weekly intervals, and QBO data were interpolated to provide consistent weekly values.

$$\begin{aligned} T(t) =& \beta_1 \cdot FS(t) + \beta_2 \cdot QBO(t) + \beta_3 \cdot \mathrm{Tlinear}(t) \\ &+ \beta_4 \cdot \sin_{\text{annual}}(t) + \beta_5 \cdot \cos_{\text{annual}}(t) \\ &+ \beta_6 \cdot \sin_{\text{semi-annual}}(t) + \beta_7 \cdot \cos_{\text{semi-annual}}(t) \\ &+ \beta_8 \cdot T_{\text{med}} + \epsilon(t) \end{aligned} \tag{1}$$

Here, T represents the temperature measured by the lidar, FS is the solar flux at 10.7 cm, QBO is the Quasi-Biennial Oscillation, Tlinear is a linear function of time specific to each time vector of the lidar studied, T_{med} is the reference temperature of the series corresponding to the median of the lidar database, and ϵ is the residual error.

In addition to these terms, we add sinusoidal terms to describe annual and semi-annual variations, with all calculations performed on day t:

$$\sin_{\text{annual}}(t) = \sin\left(\frac{2\pi t}{365.25}\right)$$

$$\cos_{\text{annual}}(t) = \cos\left(\frac{2\pi t}{365.25}\right)$$

$$\sin_{\text{semi-annual}}(t) = \sin\left(\frac{4\pi t}{365.25}\right)$$

$$\cos_{\text{semi-annual}}(t) = \cos\left(\frac{4\pi t}{365.25}\right)$$

The annual amplitude is calculated as $\sqrt{\beta_4^2 + \beta_5^2}$ and the annual phase as $\arctan(\beta_4, \beta_5)$, and the semi-annual quantities are calculated accordingly.

To account for the measurement error of the lidars, each observation is weighted by the inverse of its variance:

$$w(t) = \frac{1}{\sigma_{\text{err}}^2(t)}$$

To better understand the seasonal effects of solar or anthropogenic trends that may be different according to seasonal processes, we performed several linear regression for selected months and only concerning period either the ones identified as winter (November, December, January, February, March) or as summer time (May, June, July, August, September). For this purpose, we used Eq. (1) without the sinusoidal terms, Tlinear, and T_{med} becomes the median temperature of the database measured during the winter or summer months.

To clarify the results presented below, we have summarized two results from the linear regression in Table 1. One at an altitude of 40 km (stratosphere) and the other at 70 km (mesosphere). Each lidar calculates an average temperature based on all of its measurements, which fluctuates due to natural phenomena included in our model, annual and semi-annual variations, solar flux and QBO. Other natural factors not modeled in our regression also contribute to these variations (residuals). Finally, this average temperature changes over time, following a linear trend. Among the sources of variability in the middle atmosphere, annual seasonal cycles clearly dominate, followed by semi-annual cycles. Solar flux and QBO, on the other hand, induce variations of comparable amplitude. At the end of this table, you will also find the average measured values of solar flux and QBO used in this study.

3.3. Seasonal variations

3.3.1. Phases and amplitudes

The three lidars located at northern mid-latitudes (KUH, HOH, and OHP) show quite similar results regarding phases and amplitudes. The annual phase is situated between June and July, then drops sharply around January and February, stabilizing above 70 km. The annual amplitude follows a similar process; it is stable (≈6 to 12 K depending on the site) about 60 km, where it drops sharply close to 2 K for all three sites, then increases linearly up to the maximum altitude measured by the lidars(≈9 to 16 K depending on the site). The semi-annual phases change slowly throughout the profile from April (30 km) to July (80 km). The semi-annual amplitudes are stable between 30 and 50 km around 1.5 K, then increase linearly up to 65 km where we find a peak of (≈5 to 6 K depending on the site), before decreasing again to stabilize around 1 K. For a better understanding, you can find the results with respect to OHP in Fig. 2.

Additionally, the PCL lidar, located at the same latitude as OHP but in a very different geographical area, exhibits similar behavior with the same phases but with an annual amplitude that is approximately 1.5 K stronger. It follows the same pattern except that the amplitude decreases after 76 km. The semi-annual amplitude shows a first peak at 60 km with 5 K, and a second peak at 80 km with 7 K.

We then have measurement sites on each of the tropics thanks to MLO (north) and RUN (south). Both sites show similar amplitude values but different phases. Although they exhibit similar behavior to the lidars further north, their amplitudes are weaker. For RUN, we see a first peak of almost 3 K at about 40 km and a second one of 6 K at 75 km, for the semi-annual amplitude, the altitudes at which the peaks are located are very close together, but the amplitude is halved. The annual amplitude of MLO oscillates less; Up to 40 km, it is approximately 2.5 K, then decreases before increasing again with a peak of 4.5 K at 70 km. The semi-annual amplitude oscillates between around 1.75 K throughout the profile. The annual phase of RUN is very variable, fluctuating from September to July throughout the profile, but mainly

Table 1
Average temperature measured by lidar : T_{moy}
Variation explained by the linear regression model around T_{moy} :
• ±Ann, ±Semi
• $\pm F_{10.7}$
• ±QBO
Remaining variation around the mean that is not explained by the linear regression model :
• ±Résid
Linear change in average temperature per decade :
• Trend
Solar flux and average QBO measured during the study for each lidar :
RUN : $F_{10.7}$ = 94 SFU, QBO = 17 m/s; MLO : $F_{10.7}$ = 89 SFU, QBO = 16 m/s; TMF : $F_{10.7}$ = 104 SFU, QBO = 16 m/s; OHP : $F_{10.7}$ = 100 SFU, QBO = 18 m/s; HOH : $F_{10.7}$ = 101 SFU, QBO = 17 m/s; PCL : $F_{10.7}$ = 107 SFU, QBO = 18 m/s; ALO : $F_{10.7}$ = 86 SFU, QBO = 15 m/s; KUH : $F_{10.7}$ = 85 SFU, QBO = 14 m/s; COR : $F_{10.7}$ = 87 SFU, QBO = 14 m/s.

Lidar	T_{moy} (K)	±Ann (K)	±Semi (K)	$\pm F_{10.7}$ (K)	±QBO (K)	±Résid (K)	Trend (K/dec)
Altitude : 40 km							
Groupe 1							
RUN	253	2.83	0.64	1.76	0.13	3.18	−1.32
MLO	252	2.01	1.73	0.31	0.26	2.06	−0.56
TMF	252	6.05	0.39	0.14	0.58	2.92	−1.91
Groupe 2							
OHP	254	6.40	2.36	0.13	1.42	5.42	−0.82
HOH	253	7.66	2.25	0.11	0.06	5.52	−0.40
PCL	255	10.49	1.32	1.78	0.05	3.01	−1.61
Groupe 3							
ALO	254	16.18	4.06	1.02	0.90	8.64	−0.99
KUH	257	11.80	0.39	1.37	0.29	4.12	2.43
COR	254	16.89	4.47	–	0.77	4.62	−0.22
Altitude : 70 km							
Groupe 1							
RUN	213	3.97	2.01	0.60	0.66	6.02	−5.41
MLO	212	3.87	1.89	0.15	0.26	3.91	−0.32
TMF	214	11.15	3.02	1.75	0.17	5.38	−2.41
Groupe 2							
OHP	215	7.07	3.73	0.51	0.20	6.63	−0.89
HOH	212	6.65	3.93	1.88	0.07	6.66	−3.86
PCL	208	12.57	0.75	0.30	0.34	4.54	−2.95
Groupe 3							
ALO	221	12.43	4.02	0.59	1.80	9.91	4.22
KUH	216	12.55	2.39	0.86	0.36	5.40	1.14
COR	219	9.48	4.68	–	0.07	5.61	4.24

situated between December and January. The semi-annual phase is more stable; it drops linearly from December to January throughout the profile with two inversions: one between 33 and 42 km in August, and one between 48 and 52 km in November. The annual and semi-annual phases of MLO change linearly throughout the profile almost in the same way; for the annual, it goes from June to January, while for the semi-annual, it goes from August to March.

The TMF lidar, located between the northern and tropical regions, exhibits intermediate behavior. Its phases are similar to those of the lidars located in the northern regions, while its amplitudes lie between those of the northern and tropical lidars.

Furthermore, the ALO lidar, located at a polar latitude, shows the same phase behavior as the northern lidars and exhibits the same amplitude behavior as PCL but much stronger like a maximum value of 35 K for the annual amplitude and 14 K for the semi-annual.

Finally, the COR lidar, located at high latitude in the southern hemisphere, shows the same behavior as those in the northern hemisphere, but with a 6-month shift for the annual phase and a 3-month shift for the semi-annual phase. The annual and semi-annual amplitudes also change strongly in the stratosphere, with respective values of 16 K between 30 and 44 km for the annual, and 5 K between 35 and 50 km for the semi-annual.

The phases and amplitudes of the MSIS and ERA5 models are generally very close to the results obtained from the lidars (± one month; ±1 K), except in specific cases or at certain altitude points, such as during the RUN phases, where the differences can be more significant. You will find the phases and amplitudes of all lidars in Appendix 4.

3.3.2. Average monthly temperature

We conducted a monthly average of temperature measurements for all lidars to analyze the general behavior of the middle atmosphere over a year. Once again, we can distinguish three groups of lidars: those positioned in the mid-to-high latitude zones of the northern hemisphere, the tropical lidars, and the high-latitude southern lidar. We also note the behavior of TMF, which is situated midway between the northern and tropical lidars due to its position.

The mid-latitude northern lidars exhibit a mesosphere that expands during the summer months, with the stratopause descending in altitude and the mesopause rising. It is also noted that they have only one peak of maximum temperature around 49 km in June. In the mesosphere, the minimum temperature is found slightly offset by one month compared to the stratosphere's peak, at the measurement limit of the lidars. The temperature variation measured by OHP and HOH is the same: it is minimal during the summer and increases as winter sets in the stratosphere, as you can see in Fig. 3. The behavior is reversed in the mesosphere, with a peak variation in winter and a slight decrease during the summer. KUH, for its part, also shows the lowest variations in winter in the stratosphere, but this continues into the mesosphere. Our only lidar in the northern polar position, ALO, shows the same behaviors as the mid-latitude lidars but with a greater range of variability, which is, for example, twice as high compared to OHP.

The atmosphere measured at the southern position by the COR lidar behaves in the same manner as the northern position but with a 6-month shift.

The middle atmosphere measured by the tropical lidars is less variable. The stratosphere and mesosphere exhibit small variations in altitude, and we find multiple peaks of maximum temperatures in the stratosphere in April and October for MLO, and in December and May for RUN. It is also noted that the temperature changes much less in the stratosphere of tropical regions than in mid-latitude regions. The same goes for the mesosphere, with a minimal peak in May for MLO and two peaks in April and October for RUN. Note that RUN measures 10 km higher than MLO, and it is perhaps for this reason that we find only one peak on MLO. The variations are maximal during winter on both sites in the stratosphere and are rather homogeneous throughout the year in the mesosphere. They are also more significant than in the stratosphere. You will find the monthly median temperature of all lidars in Appendix 1.

3.3.3. Comparison with models

All sites show similar behavior compared to ERA5, with very small differences, whether in relation to monthly medians or concerning monthly variability up to 50 km. Beyond this altitude, as no more data is assimilated into the model (section 1.2), measurement differences as well as atmospheric variability begin to increase, reaching up to 30 K difference in monthly medians. Additionally, the model is systematically colder than the lidar measurements as you can see in Fig. 4. The comparisons of all monthly median temperatures between Lidar and ERA5 can be found in Appendix 2 (Mariaccia et al., 2022).

Unlike ERA5, MSIS, being a purely mathematical model based on observations, shows variations in differences between monthly values that depend more on the sites and across the entire profile. The differences can sometimes be small, as for the MLO site, where they range from −3 to +5 K, but they can also be much larger, as for the KUH site, where they range from −10 to +35 K. Although the differences

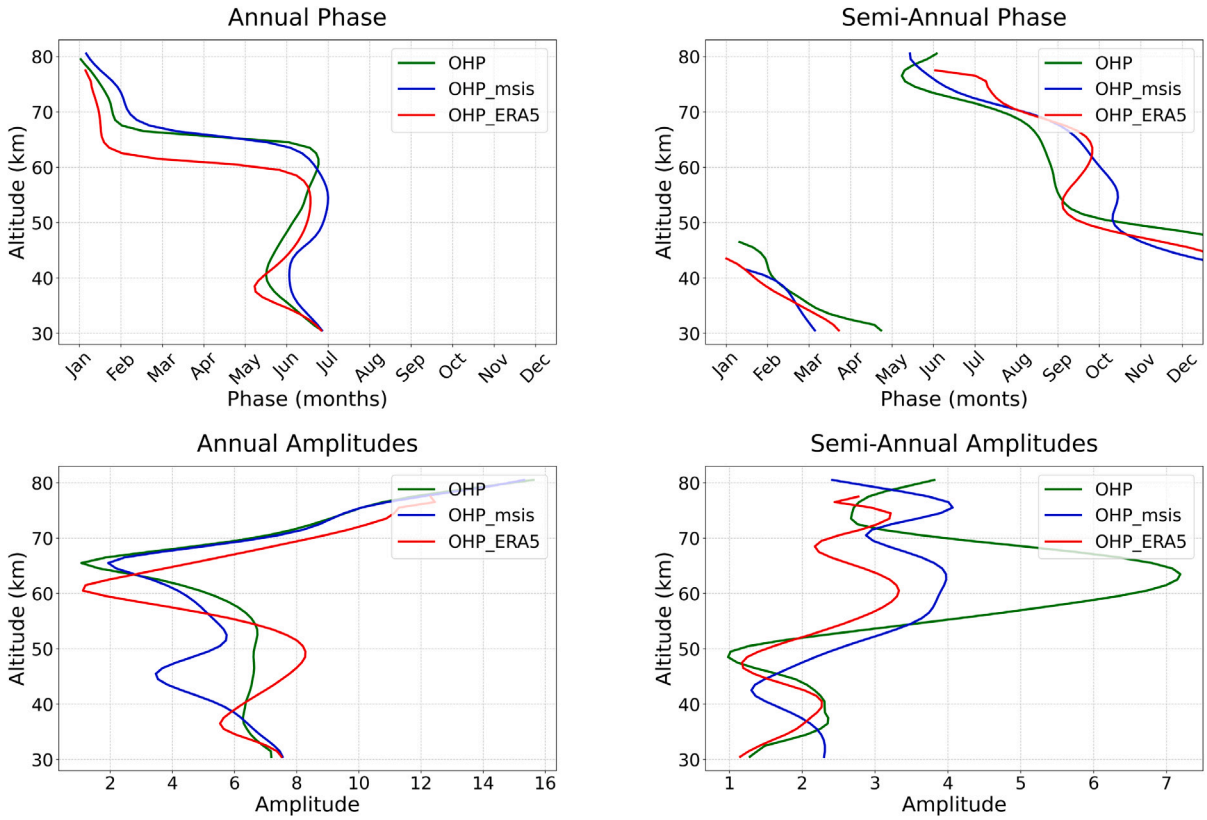

Fig. 2. Annual and semi-annual phase and amplitude values for the OHP site.

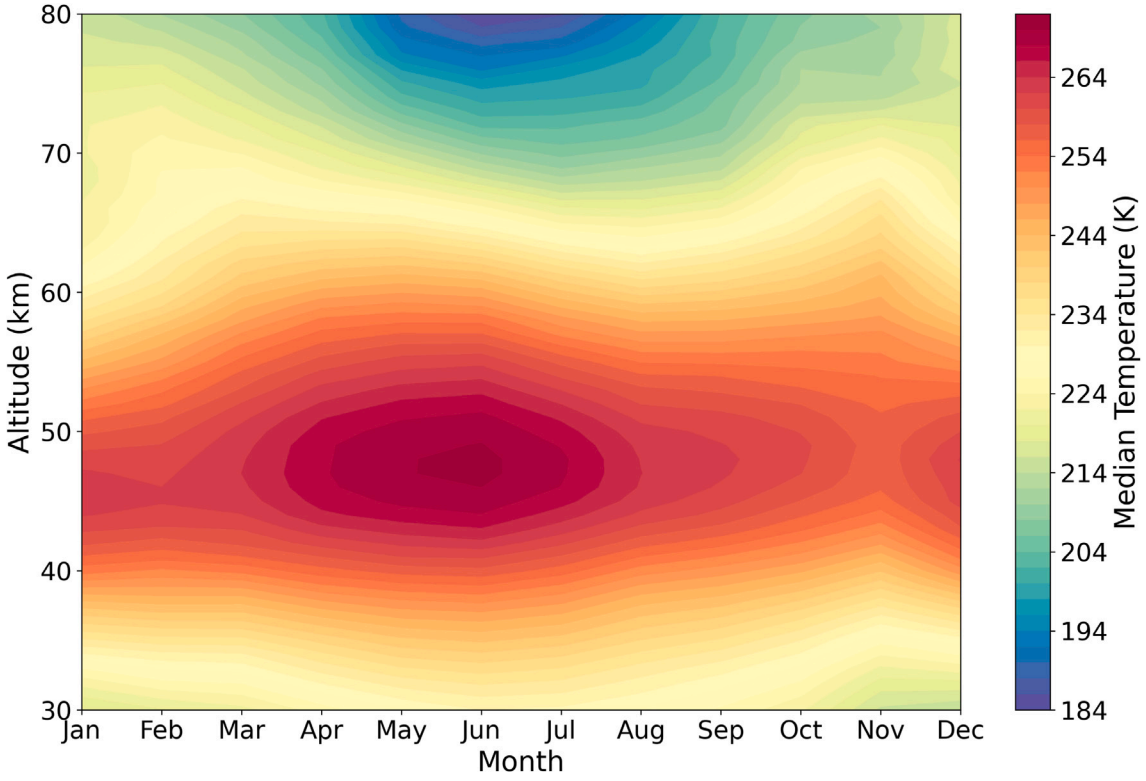

Fig. 3. Monthly median temperature map at the OHP site.

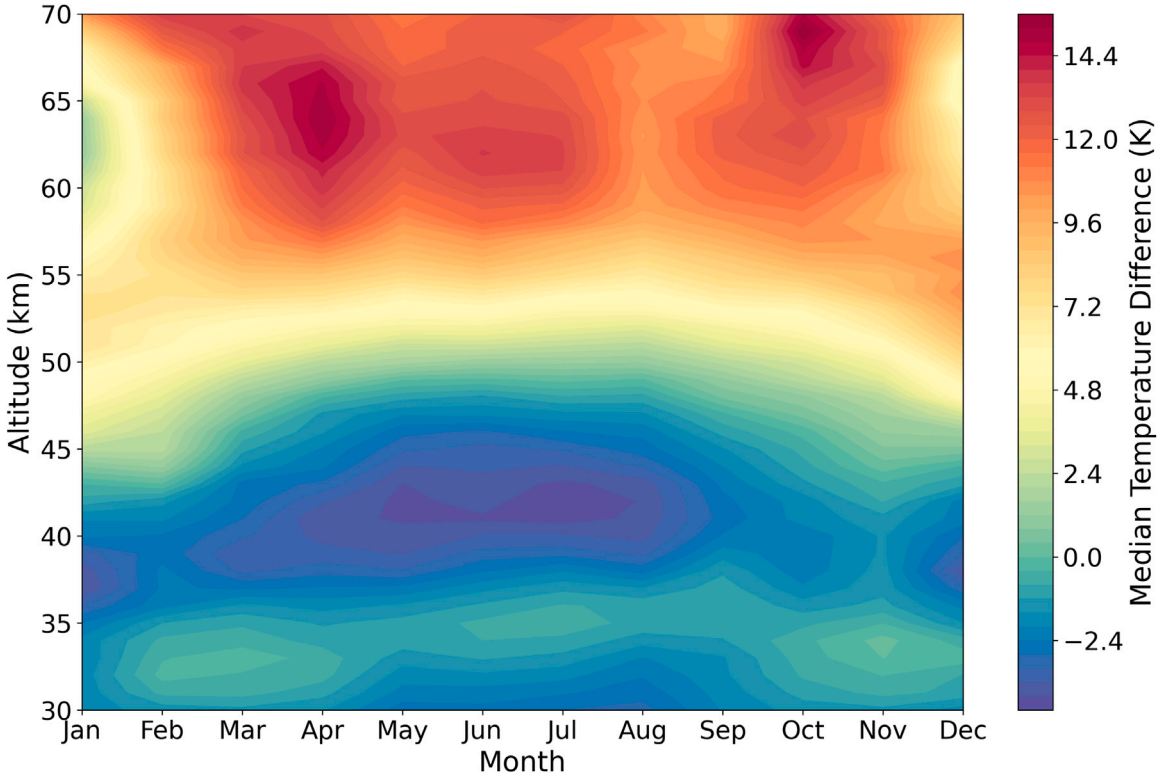

Fig. 4. Map of monthly median temperature differences between lidar and ERA5 at the OHP site.

compared to lidar measurements seem more random when compared to the ERA5 model, certain systematic effects are noted, such as greater variability in the mesosphere compared to the stratosphere and during the transition phases of spring and autumn. Fig. 5 shows an example of a comparison made with the OHP Lidar. The comparisons of all monthly median temperatures between Lidar and MSIS can be found in Appendix 3.

4. Inter-annual variability

For the analysis of interannual variability, the results are examined in three distinct groups based on latitude. The first group includes lidars in tropical positions: RUN, MLO, and TMF. As already mentioned, TMF lidar has a special position, as it is centrally located between the tropics and mid-latitudes. The second group consists of lidars in mid-latitude positions: OHP, HOH, and PCL. The third group comprises lidars in polar and near-polar regions: ALO, KUH, and COR. It should be noted that all uncertainties in the estimation of each proxy presented here are given at 1 sigma via the weighted least squares (WLS) regression model weighted by the lidar error. These uncertainties can be used because, as explained in Section 3.2, averaging the data over a week allows us to avoid autocorrelation.

4.1. Response to fluctuations in solar activity

4.1.1. Lidar results

To obtain the average temperature variations due to solar activity fluctuations in the middle atmosphere, we multiply the coefficient obtained from the linear regression by the median of the average solar flux measured over the lidar study period.

The first group, located in tropical and subtropical regions, shows a variation centered on 0 K, oscillating between −2 K and 2 K. The particular situation of TMF indicates that it does not behave exactly like the tropical sites, as it does not seem to vary around 0 K but rather shows a positive correlation with altitude, ranging from 0 K at 30 km to nearly 2 K at the top of the profile at 70 km, approaching the signatures obtained above mid-latitude sites. The second group displays more significant variations than in the tropics, with a rather negative amplitude in the stratosphere going down to −2 K and a rather positive signature in the mesosphere with an amplitude up to +4 K. It is noted that PCL exhibits the largest variation amplitude in the group. This type of signature has already been observed when the series were shorter (Keckhut et al., 2005). For the third group, we observe even higher amplitudes than in the tropics and greater variability than the previous two groups. The minimum amplitude is −3 K, and the maximum amplitude is 3 K. For KUH and ALO, we find the same type of profiles as in the tropics, with a kind of oscillation around a reference value, but this time the oscillation is not around 0 K but around −2 K for ALO and 2 K for KUH. Since the COR series does not yet span more than one full solar cycle, the solar flux component was not integrated into the linear regression (Fig. 6).

It is important to note that the most significant fluctuation on the timescales of the series studied is the 11-year solar cycle. Consequently, some sites have not yet measured a complete cycle, which poses a significant challenge in distinguishing between solar activity and anthropogenic variations (Kerzenmacher et al., 2006). The number of solar cycles covered by each site is represented in Fig. 7.

4.1.2. ERA5 comparisons

As in Section 4.1.1, to compare the average effects of the solar flux found by ERA5 and lidar on the average atmosphere, we multiply the coefficients obtained by the average solar flux measured over the period studied. It is very interesting to note that comparisons with ERA5 show that the model, when extrapolated above the lidar sites, correctly accounts for variations related to solar flux. When we compare the average variations measured by the lidars with those measured by ERA5, the difference is almost always very small across nearly all sites. The maximum values rarely reach 0.02 K, with one exception: ALO between 30 and 40 km, where the maximum negative values reach 0.06 K (Fig. 8).

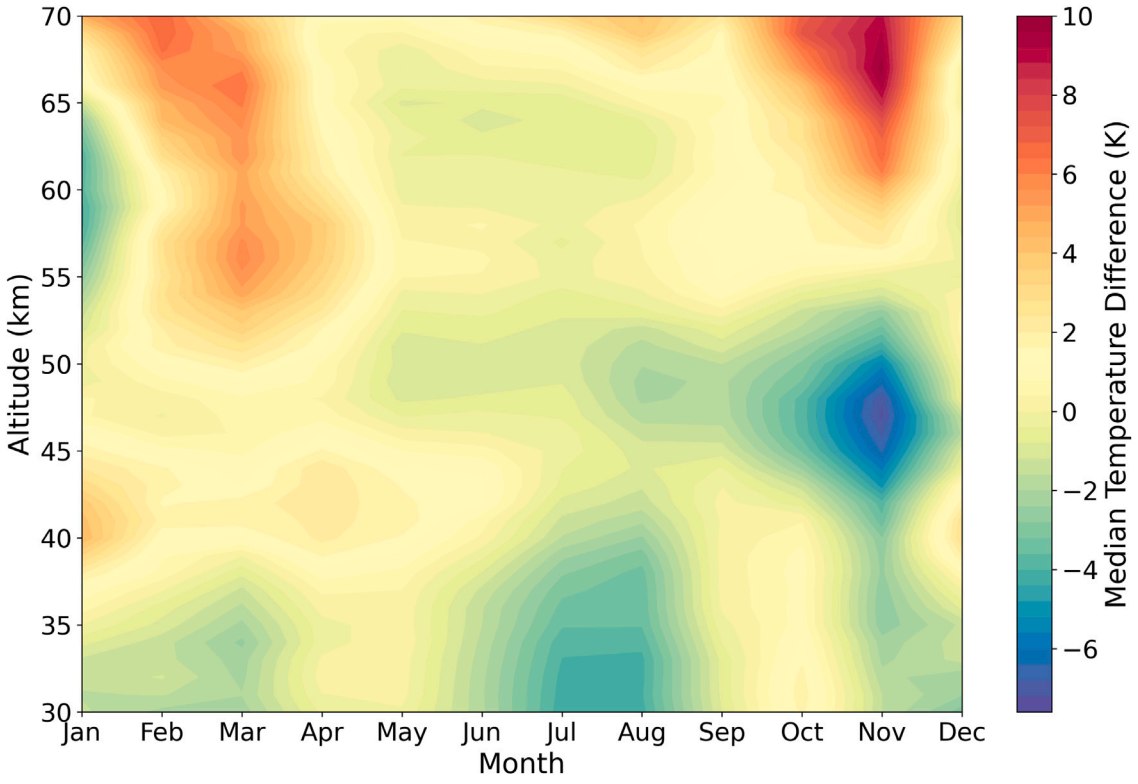

Fig. 5. Map of monthly median temperature differences between lidar and MSIS 2.0 at the OHP site.

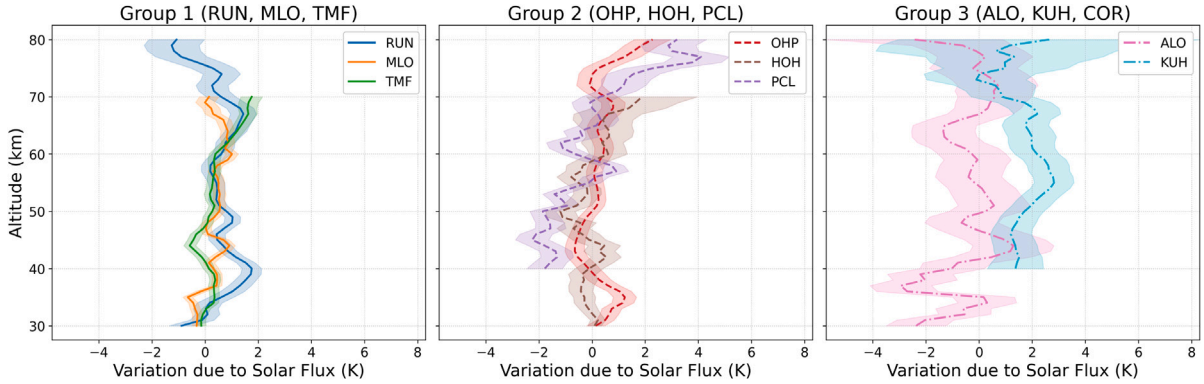

Fig. 6. Temperature variation due to the solar cycle in the middle atmosphere. The right figure represents tropical lidars, the center represents mid-latitude lidars, and the last figure represents polar or near-polar regions. Uncertainties are shown at 1 sigma.

4.1.3. Winter/summer

To better understand the behavior of the middle atmosphere throughout the year, we applied our linear regression to the winter and summer months separately. Previous investigations had shown that solar fluctuations could induce effects on the dynamics and create signatures of dynamic origin. It is noteworthy that the amplitude of the impact of solar flux variations on the temperature variations of the middle atmosphere is greater in winter than in summer, except for the tropical lidars where the results are similar. The range of maximum fluctuations measured during winter is about 10 K across all combined results, whereas the range of fluctuations in summer does not exceed 5 K. In summer at low and mid-latitudes, the responses are very weak, while in winter we find more clearly this anti-correlation between the stratosphere (with a negative response) and the mesosphere positive response; results in good agreement with previous modeling studies that showed that even weak effects at the tropics modulate the appearance of stratospheric warmings (Hampson et al., 2005; Marchand et al., 2011).

In summer, however, we expect a maximum photochemical effect in the tropics in the upper stratosphere but less than 1 K (Hood et al., 1993a,b), which explains why the average results are close to this value. Only the site at La Réunion shows a slightly stronger signal (Fig. 9).

4.2. Atmospheric response to the QBO

4.2.1. Lidar results

To obtain the average temperature variations due to QBO in the middle atmosphere, we multiply the coefficient obtained from the linear regression by the median of the QBO measured over the lidar study period.

It is observed that, for the majority of sites, the average influence of the QBO on temperature remains weak, oscillating around 0 K. However, a notable peak appears in the stratosphere with an amplitude sometimes exceeding 1 K depending on the site, which corresponds to

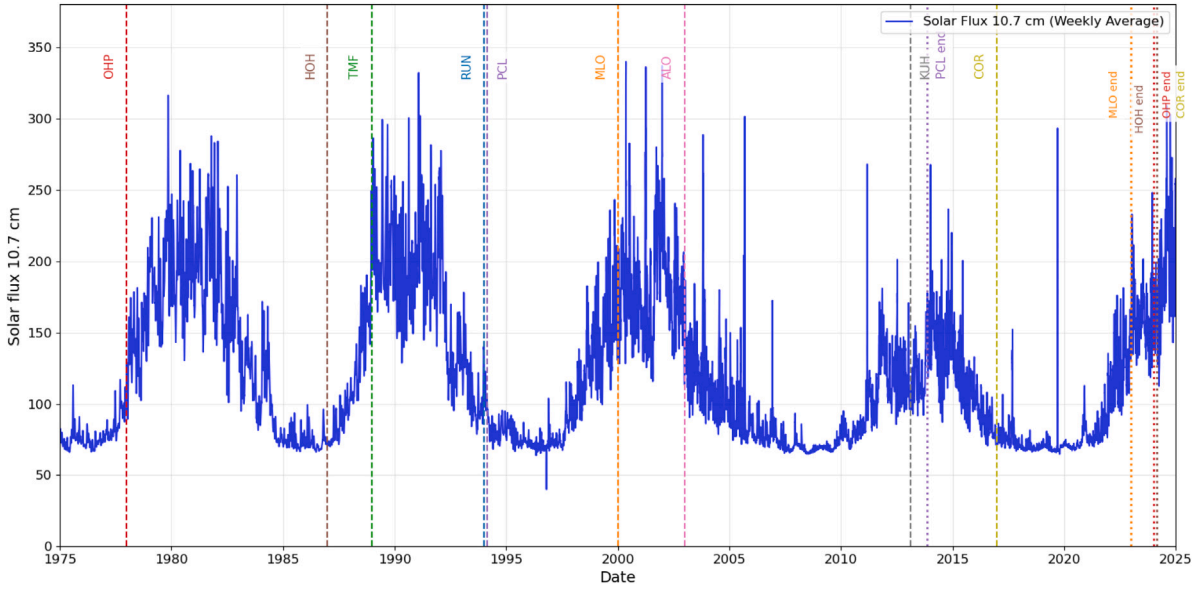

Fig. 7. In blue the weekly solar flux measurements at 10.7 cm used in this study. The dashed lines indicate the start of each lidar measurement, if a measurement ends before the end of the figure, this is indicated by a dotted line.

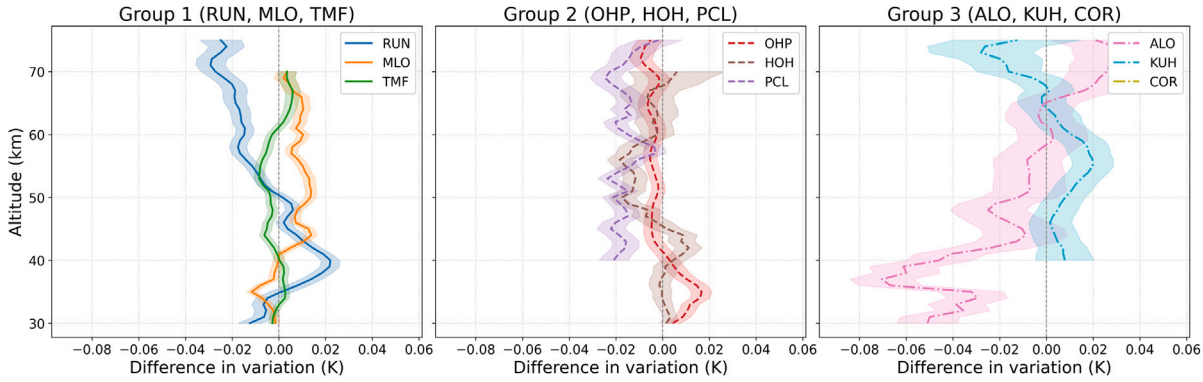

Fig. 8. Difference in temperature variation profiles due to solar flux measured by lidars and modeled by ERA5 (Lidar – ERA5). The uncertainty of this comparison is displayed at 1 sigma.

expected results as shown by Martin et al. (2020) and Huang et al. (2006). Another trend that seems to emerge is that this peak is always positive in the northern hemisphere, whereas it would be negative in the southern hemisphere. For the case of ALO, a much more significant effect is noted, ranging from −3 K to 2 K, occurring throughout the profile. These results are due to the interaction between the QBO and the measured polar vortex (Yamazaki et al., 2020) (Fig. 10).

4.2.2. ERA5 comparisons

As in Section 4.2.1, to compare the average effects of the QBO found by ERA5 and lidar on the average atmosphere, we multiply the coefficients obtained by the average QBO measured over the period studied. Just like with solar flux, ERA5 appears to model variations due to the QBO very well. The difference between the average variation profiles due to the QBO measured by the lidars and those modeled by ERA5 rarely exceeds 0.1 K as show in the Fig. 11.

4.2.3. Winter/summer

As with solar flux, to better understand the behavior of the middle atmosphere throughout the year, we applied our linear regression to the winter and summer months only. Since the propagation of planetary waves is strongly influenced by the QBO (Holton and Tan, 1980), as expected, the maximum extent of the temperature response is greater in winter than in summer. In winter, the value is approximately 3 K (except for ALO), whereas in summer, it is below 1 K except for RUN. We also note the interaction between the polar vortex and the QBO at the ALO site, where variations in summer are almost negligible, while in winter, the maximum amplitude reaches 6 K (Fig. 12).

4.3. Linear response

The results regarding the linear response over the entire duration of lidar observations show a cooling trend at tropical, subtropical, and mid-latitude sites, which increases with altitude. The cooling is approximately 1 K per decade in the stratosphere and increases up to 2 K per decade in the mesosphere. The highest cooling is observed at the RUN sites with more than 5 K per decade. However, at sites near the polar circle and polar regions, a warming of the middle atmosphere of about 2 K per decade is observed (Fig. 13). Above 70 km, the variability is higher, and the results are likely less significant. For COR, the uncertainty in the linear response is still too high to determine whether the middle atmosphere is warming or cooling. For this site, it will be important to continue regular observations for more than 5 years to have a complete solar cycle to confirm this warming trend measured by other lidars in the polar regions. These trends confirm those identified in 2020, which included various measurement methods

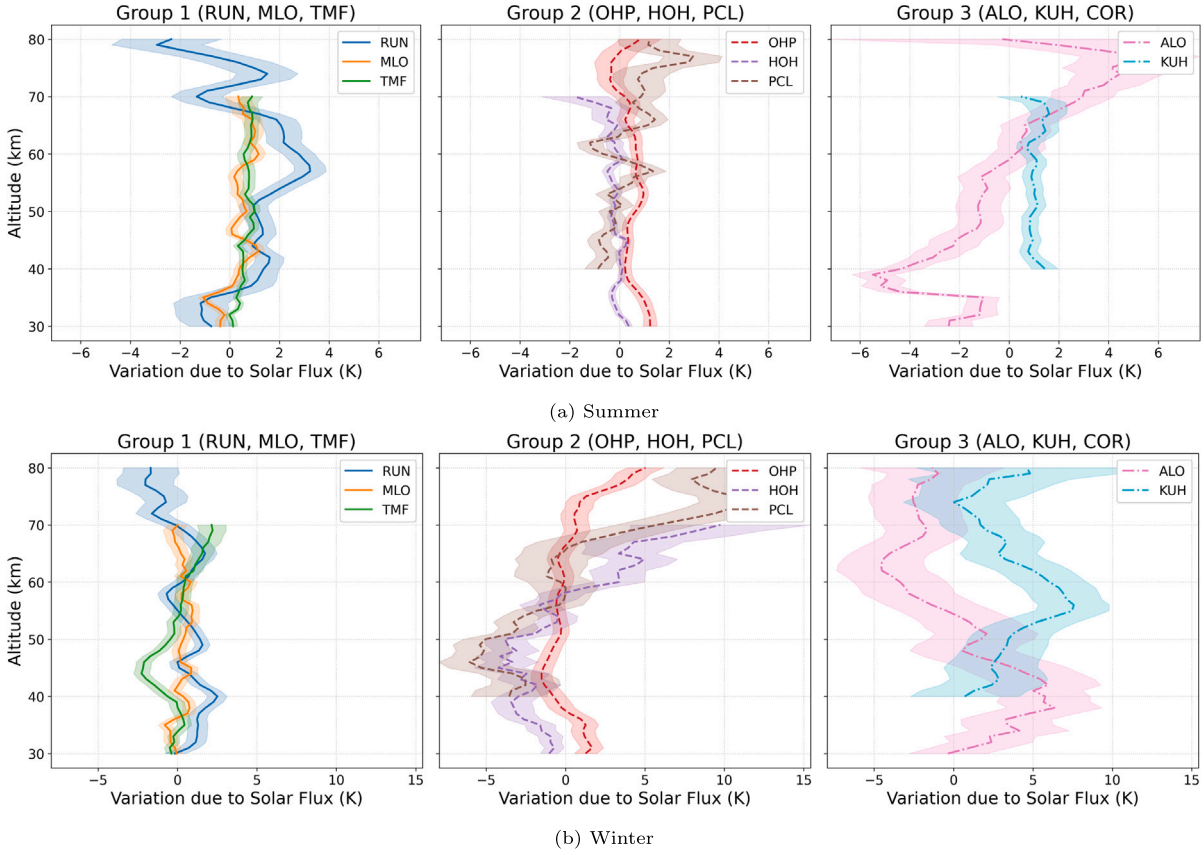

(a) Summer

(b) Winter

Fig. 9. The top figure (a) shows the results in relation to the solar flux in summer, the bottom (b) figure in winter. Winter and summer months considered: 5, 6, 7, 8, 9 and 11, 12, 1, 2, 3.

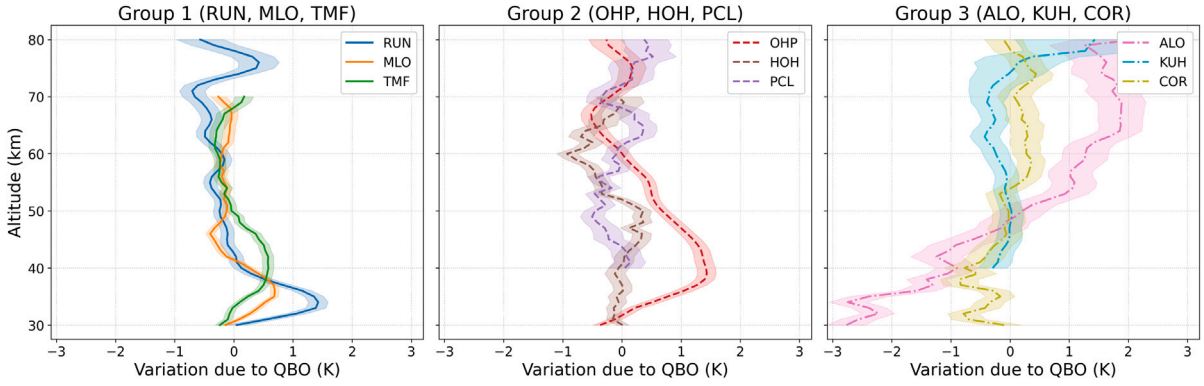

Fig. 10. Temperature variation due to the QBO in the middle atmosphere. Uncertainties are shown at 1 sigma.

of the middle atmosphere such as radiosondes, radio occultation, SSU, MSU, etc. (Steiner et al. 2020) for cooling measurements but not for the warming of polar and near-polar regions.

To confirm these warming phases occurring at some sites, we analyzed the trends to confirm the results given by the linear regression for all lidars but only from 2013 to the end of 2024. The behaviors of the different sites remain the same.

5. Analysis of residual anomalies

To verify if our proxy model accurately reproduces temperature variations in the middle atmosphere, we applied it at three different altitudes (40, 50, and 70 km) and compared it to lidar measurement data. Several observations can be made from these plots (Fig. 14). Firstly, the variability of the middle atmosphere increases as we move away from the equator, with the maximum variability observed at the polar site of ALO. Secondly, although the model agrees with the temporal evolution indicated by the succession of raw data, the model's amplitudes are much weaker. Indeed, this type of analysis does not account for rapid and local fluctuations associated with dynamics such as gravity waves, which can be a significant source of variation in the middle atmosphere from one site to another and from one period to another. Thirdly, there is a shift between the modeled temperatures and the measured temperatures at the KUH, ALO, and RUN sites; this is due to the fact that the database predominantly contains measurements from summer/winter, and this point can be easily corrected by calculating a weighted average or by applying linear regression to monthly average values. However, this representation has the advantage of

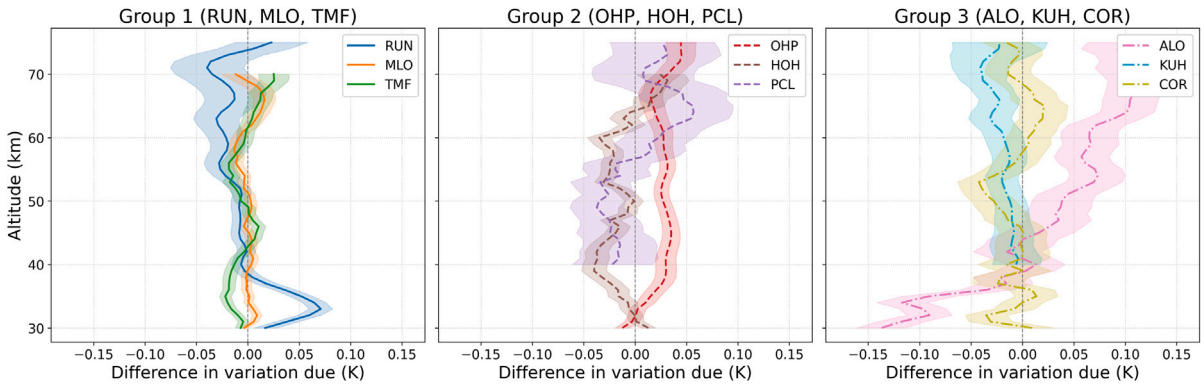

Fig. 11. Difference in temperature variation profiles due to QBO measured by lidars and modeled by ERA5 (Lidar – ERA5). The uncertainty of this comparison is displayed at 1 sigma.

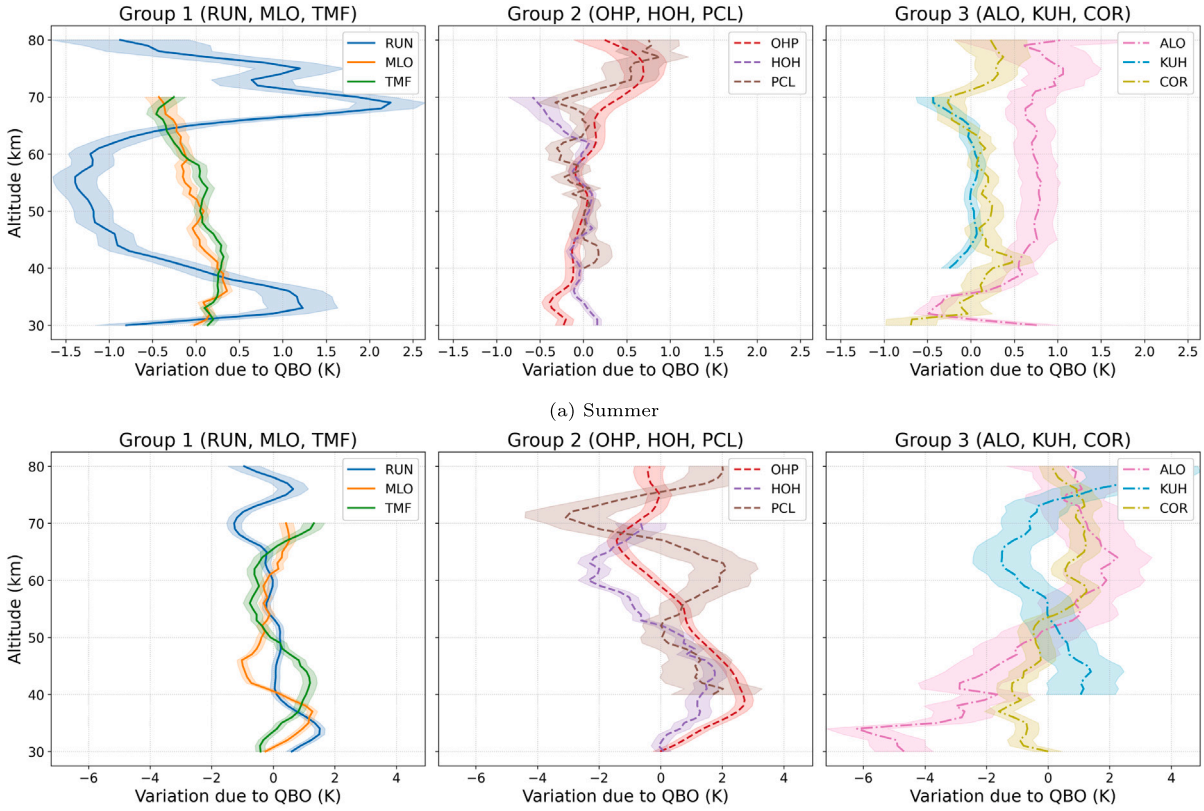

(a) Summer

(b) Winter

Fig. 12. The top figure (a) shows the results relative to the QBO in summer, the bottom figure (b) in winter. Winter and summer months considered: 5, 6, 7, 8, 9 and 11, 12, 1, 2, 3.

showing the temporal coverage of observations, the variability over time, and from one site to another. For all sites covering a period of one or more solar cycles, evident trends appear. The precise quantification of these trends depends on considering other causes of interannual variations, particularly variations in solar activity, which can interfere with the linear response estimates depending on the start and end dates of the series relative to the solar cycle.

6. Conclusion

Using long-term temperature datasets obtained with Rayleigh lidars at nine different locations within the NDACC MLO, Hawaii (19.5°N); TMF, California (34.4°N); OHP, France (43.9°N); RUN, La Réunion (21.1°S); HOH, Germany (47.8°N); PCL, Canada (42.5°N), and contributing to the ARISE project (ALO, Norway (69.3°N); KUH, Germany (54.1°N); COR, Argentina (53.7°S), we studied the temperature of the middle atmosphere by analyzing the effects of changes in solar activity, oscillations associated with the QBO, and seasonal phenomena represented by annual and semi-annual sinusoidal signals on temperature variations. This also allowed us to deduce the continuous evolution of the average temperature over time, which could be induced by the decrease in stratospheric ozone and the increase in greenhouse gases. Seasonal variations (solar flux, QBO, annual and semi-annual cycles) are generally well reproduced by ERA5 and MSIS 2.0, with results close to lidar measurements. However, some divergences persist:

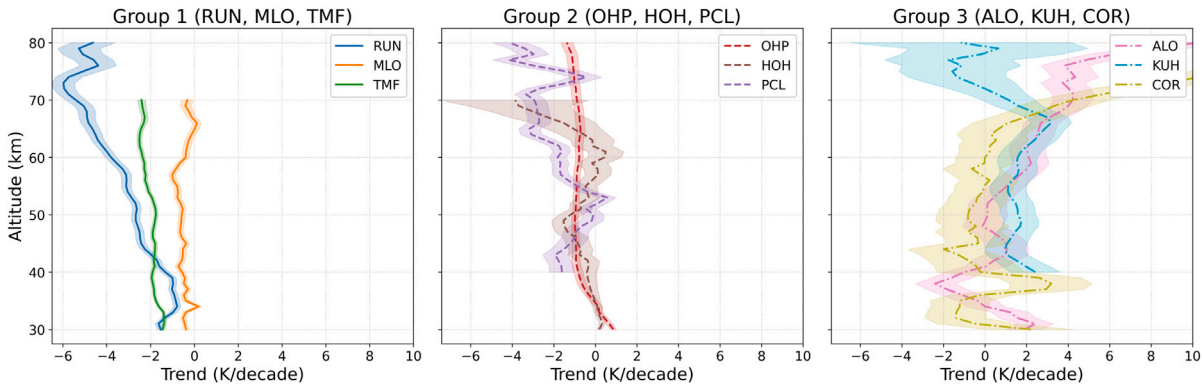

Fig. 13. Trend values in K/decade for each lidar position. Uncertainties are shown at 1 sigma.

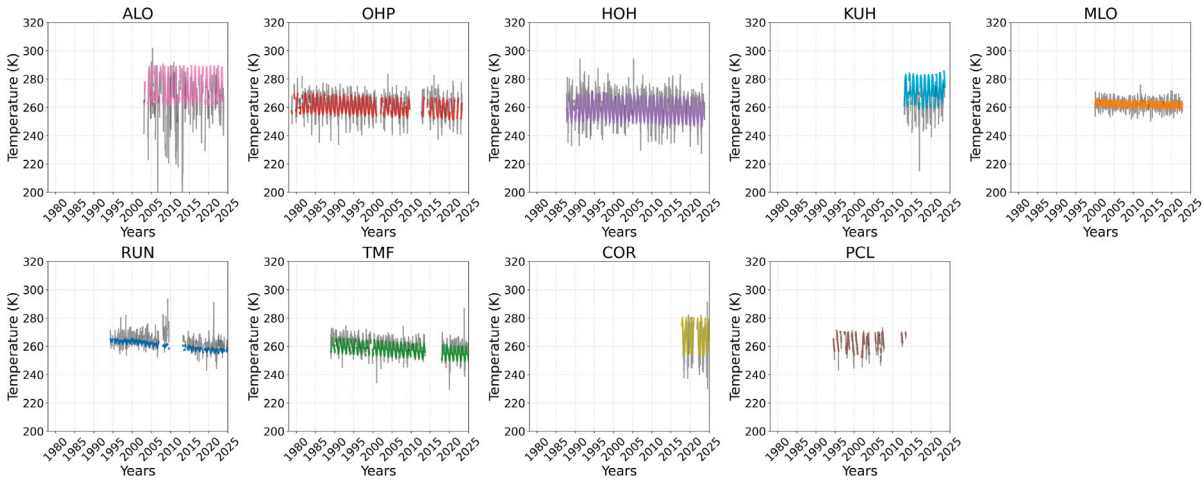

Fig. 14. Anomalies of the different lidar sites at 50 km. In gray the raw values measured by the lidars and in color the values returned by the linear regression.

- ERA5 systematically shows a colder mesosphere beyond 50 km (differences up to 20 K).
- MSIS shows significant spatial variability, with extreme differences (e.g., +35 K at KUH compared to +5 K at MLO).

Neither model clearly identifies trends in the middle atmosphere. The average temperature variation induced by solar flux differs by site, with amplitudes ranging from −2 K to +4 K. On average, these variations are around 1 K, consistent with the influence of photochemical processes in the middle atmosphere, particularly those related to ultraviolet radiation absorption (11-year cycle) and ozone dissociation. Other differences, particularly at mid and high latitudes, are mainly attributable to dynamic phenomena, as evidenced by larger amplitudes in winter than in summer. This seasonal variability suggests an important role of planetary waves and meridional circulations, which modulate the atmospheric thermal response to variations in solar flux.

The average variability associated with the QBO is generally more modest than that induced by solar flux, with generally weak amplitudes centered around 0 K, on the order of ±0.2 K. However, a peak in variation is systematically observed in the upper stratosphere, reaching about 1 K. At polar latitudes, particularly at the ALO site, the response to the QBO is much more pronounced. A quasi-linear variation in temperature is observed, ranging from a cooling of about −3 K at 30 km to a warming of +2 K at 80 km. This particular vertical structure reflects the influence of the QBO on the dynamics of the polar vortex. As with solar forcing, the effects of the QBO on the temperature of the middle atmosphere are amplified in winter. This seasonality is explained by more active dynamics and more efficient interaction between waves and general circulation, which determine how the QBO signal propagates.

A global cooling of the middle atmosphere of about −2 to −1 K per decade is observed in tropical and mid-latitude regions. In contrast, in polar and high-latitude regions, warming of about +2 K per decade is measured. The trends observed by lidars are consistent with those from other techniques such as satellites and radio occultation but show more pronounced amplitudes. This difference can be explained by the localized nature of lidar measurements, which, unlike the extensive geographic averages of other methods, more sensitively capture regional variations and dynamic or orographic effects specific to each site.

All responses are close to what we expected and exhibit a similar shape according to latitude, except for La Réunion, which provides a vertical response of seasonal, QBO and linear response differences. Although the instrument is very similar to others and has been validated through comparison with NASA instruments, it could suggest the presence of specific processes around the Indian Ocean.

This local approach thus better highlights certain climate signals, emphasizing the importance of maintaining long series of lidar measurements, in addition to global networks, to refine climate models and identify the physical processes behind the observed trends.

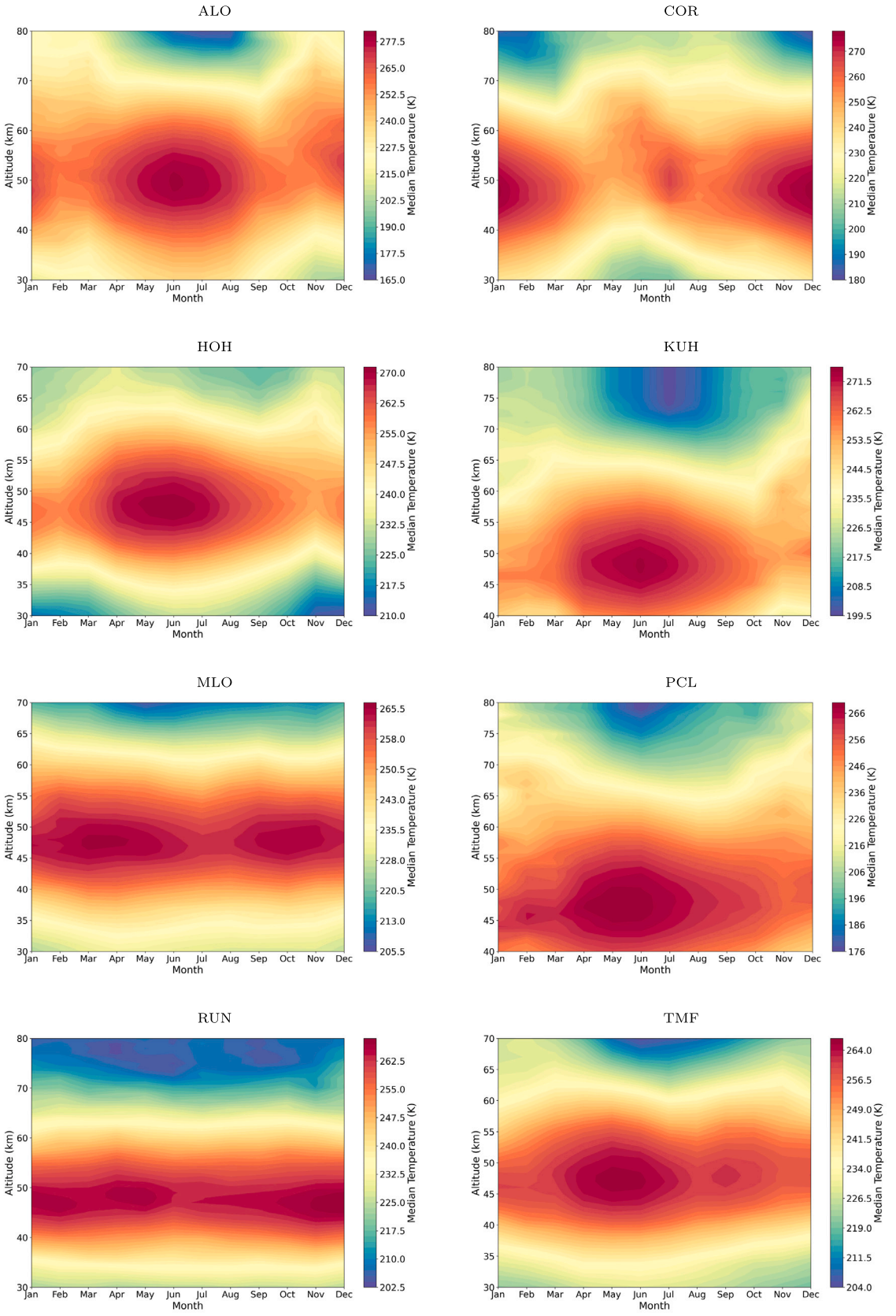

Fig. 15. Average monthly temperature for ALO, COR, HOH, KUH, MLO, PCL, RUN, TMF.

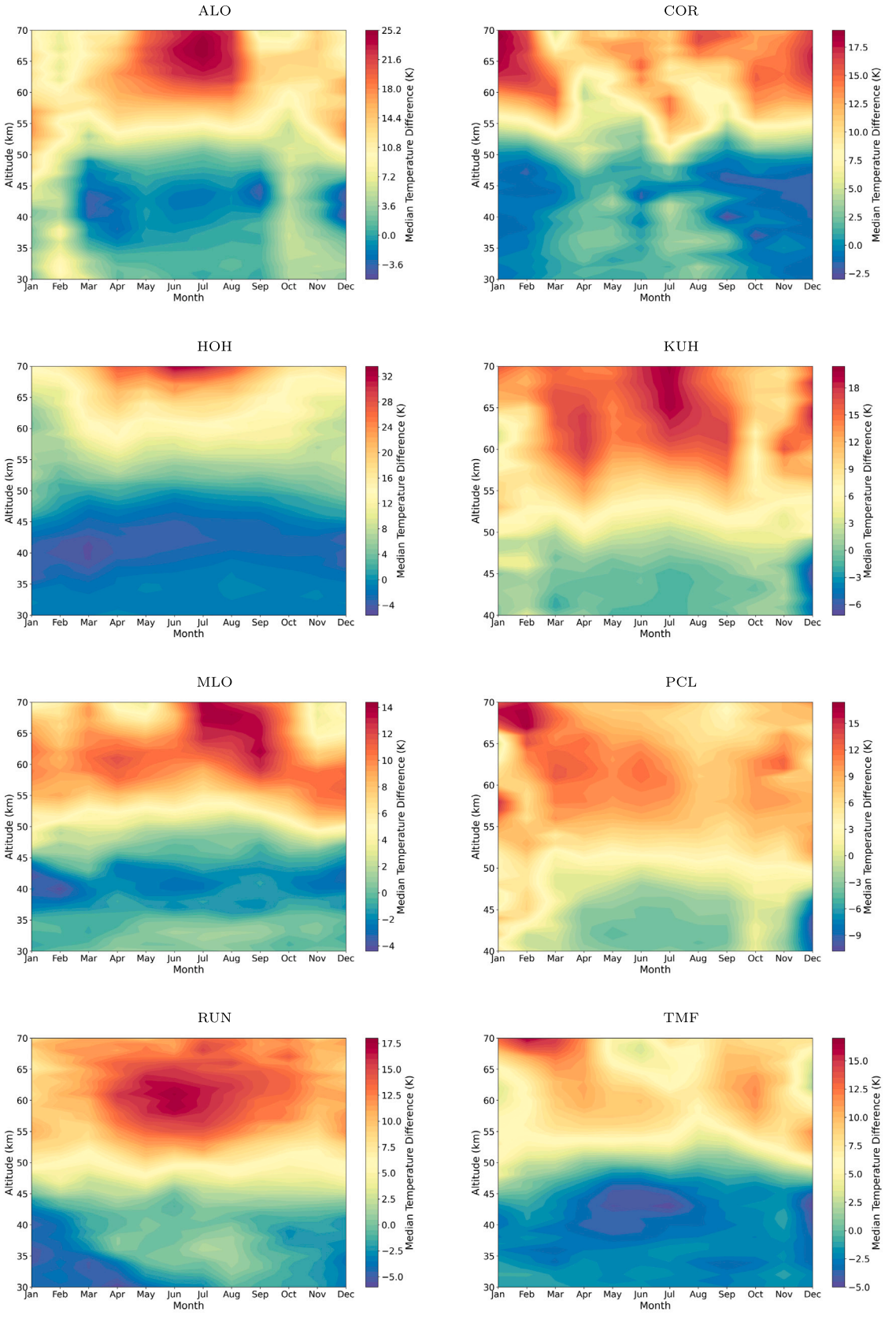

Fig. 16. Monthly median temperature differences between lidar and ERA5 for ALO, COR, HOH, KUH, MLO, PCL, RUN, TMF.

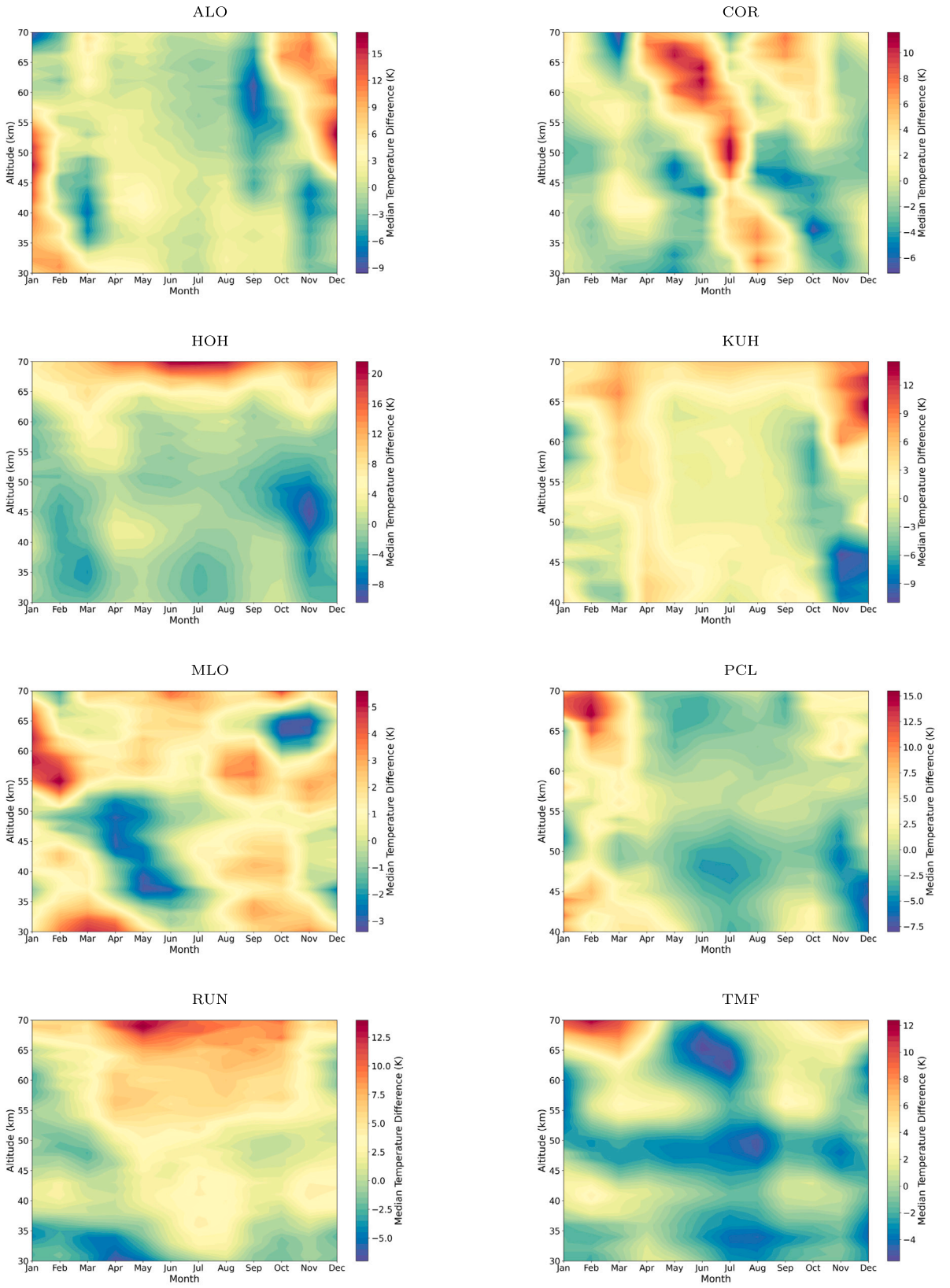

Fig. 17. Monthly median temperature differences between lidar and MSIS for ALO, COR, HOH, KUH, MLO, PCL, RUN, TMF.

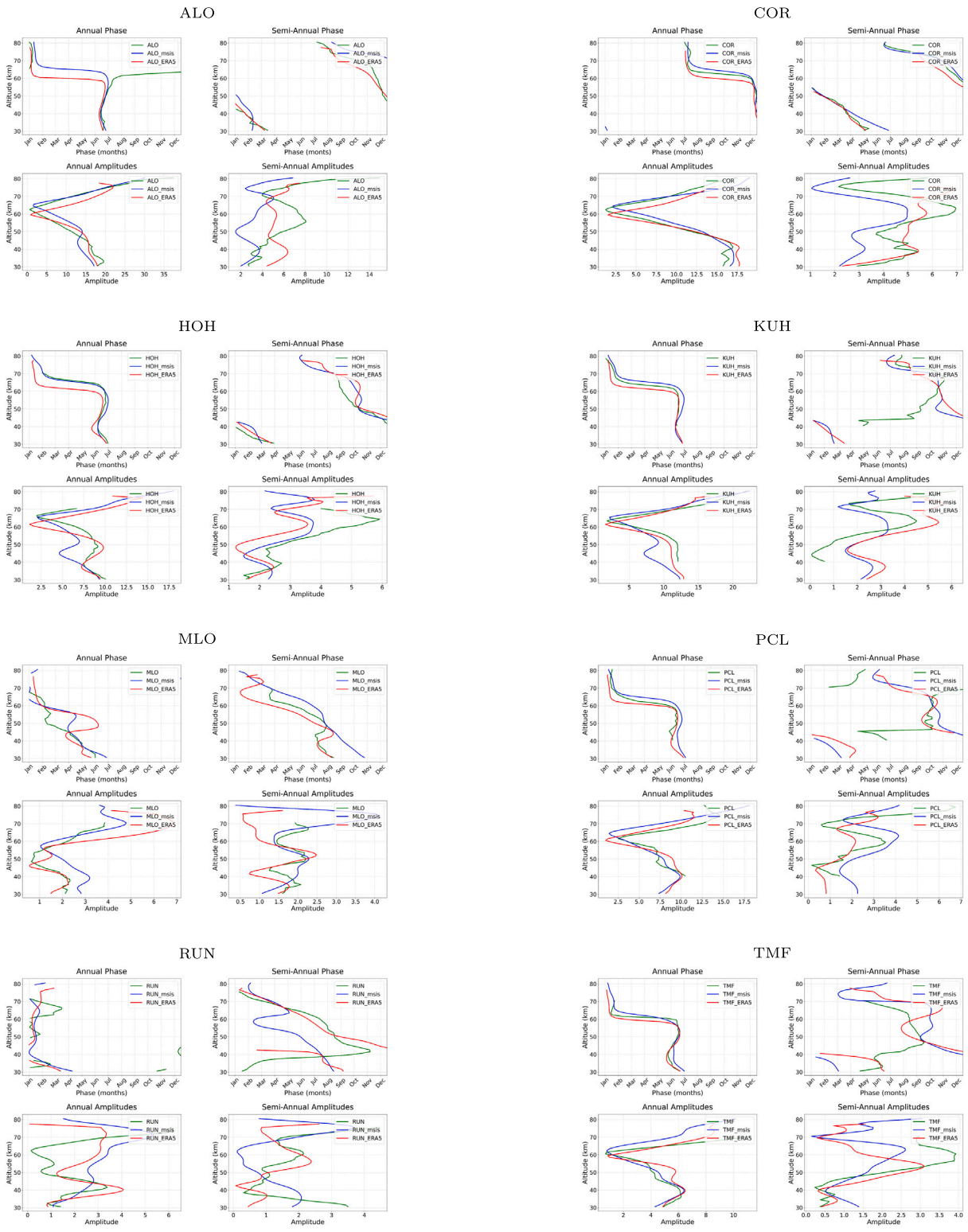

Fig. 18. Phases and amplitudes for ALO, COR, HOH, KUH, MLO, PCL, RUN, TMF.

CRediT authorship contribution statement

Pedro Da Costa Louro: Writing – original draft. **Philippe Keckhut:** Writing – review & editing. **Alain Hauchecorne:** Writing – review & editing. **Robin Wing:** Writing – review & editing. **Gerd Baumgarten:** Writing – review & editing. **Michael Gerding:** Writing – review & editing. **Thierry Leblanc:** Writing – review & editing. **Bernd Kaifler:** Writing – review & editing. **Natalie Kaifler:** Writing – review & editing. **Wolfgang Steinbrecht:** Writing – review & editing. **Ali Jalali:** Writing – review & editing. **Robert J. Sica:** Writing – review & editing.

Funding

Lidar operations are supported by CNRS, NASA, DWD, CNES, and the universities of La Réunion and Versailles Saint-Quentin-en-Yvelines. This project was carried out with the support of the Direction Générale

de l'Armement (DGA) from the French Ministry of Armed Forces under contract no. 202395002. This work also benefited from State aid managed by the French National Research Agency (ANR) under the France 2030 program, reference ANR-23-CMAS-0001.

This study is part of the preparation for the ESA mission ALTIUS, in collaboration with BIRA-IASB, with a funding contribution from CNES. The authors gratefully acknowledge ACRI-ST, without whom none of this work would have been possible (https://www.acri-st.fr/fr/).

This research was funded by Délégation Générale pour l'Armement (DGA) from the french ministry of armed force under the contrat 202395002.

Part of this research was carried out at the Jet Propulsion Laboratory (JPL), California Institute of Technology, under a contract with the National Aeronautics and Space Administration (no. 80NM0018D0004)

Declaration of competing interest

The authors declare that they have no known competing financial interests or personal relationships that could have appeared to influence the work reported in this paper.

Acknowledgments

This work was performed within the framework of the European ARISE project.

Appendix 1. Average monthly temperature

See Fig. 15.

Appendix 2. Comparison with ERA5

See Fig. 16.

Appendix 3. Comparison with MSIS

See Fig. 17.

Appendix 4. Phases and amplitudes

See Fig. 18.

Data availability

The lidar data used in this publication are publicly available as part of the Network for the Detection of Atmospheric Composition Change (NDACC). They are accessible through the NDACC international website (http://www.ndacc.org) and through the French national Centre for Atmospheric Data and Services, AERIS (https://www.aeris-data.fr/).

The ERA5 data on single levels and pressure levels were obtained from the Copernicus Climate Data Store and are available at https://cds.climate.copernicus.eu/.

The solar flux at 10.7 cm used in this study was obtained thanks to the Laboratory for Atmospheric and Space Physics (LASP) and the Interactive Solar Irradiance Datacenter (LISIRD). The data are available at https://lasp.colorado.edu/lisird/data/penticton_radio_flux.

The Quasi-Biennial Oscillation (QBO) dataset provided by the Karlsruhe Institute of Technology (KIT) is available at https://www.atmohub.kit.edu/english/807.php.

The MSIS model, supported by the Office of Naval Research and NASA, is available at https://ccmc.gsfc.nasa.gov/models/NRLMSIS~2.0/.

The Hohenpeissenberg lidar data is available at https://dx.doi.org/10.60897/x48r-e929.

The CORAL lidar data is available at https://doi.org/10.5281/zenodo.17241353. Kaifler, B., & Kaifler, N. (2025). Middle atmosphere temperature profiles by the CORAL lidar at Rio Grande, Southern Argentina.

The DOI 10.22000/fncjgk3afh2qt1dw will be activated after acceptance of the paper. The final version of the text (after acceptance) will only refer to the DOI.

References

Angot, G., Keckhut, P., Hauchecorne, A., Claud, C., 2012. Contribution of stratospheric warmings to temperature trends in the middle atmosphere from the lidar series obtained at Haute-Provence Observatory (44° n). J. Geophys. Res. Atmospheres 117 (D21), http://dx.doi.org/10.1029/2012jd017631.

Baldwin, M.P., Gray, L.J., Dunkerton, T.J., Hamilton, K., Haynes, P.H., Randel, W.J., Holton, J.R., Alexander, M.J., Hirota, I., Horinouchi, T., Jones, D.B.A., Kinnersley, J.S., Marquardt, C., Sato, K., Takahashi, M., 2001. The quasi-biennial oscillation. Rev. Geophys. 39 (2), 179–229. http://dx.doi.org/10.1029/1999rg000073.

Baray, J.-l., Courcoux, Y., Keckhut, P., Portafaix, T., Tulet, P., Cammas, J.-p., Hauchecorne, A., Beekmann, S.G., De Mazière, M., Hermans, C., Desmet, F., Sellegri, K., Colomb, A., Ramonet, M., Sciare, J., Vuillemin, C., Hoareau, C., Dionisi, D., Duflot, V., Vérèmes, H., Porteneuve, J., Gabarrot, F., Gaudo, T., Metzger, J.-m., Payen, G., De Bellevue, J.L., Barthe, C., Posny, F., Ricaud, P., Abchiche, A., Delmas, R., 2013. Maïdo observatory: a new high-altitude station facility at Reunion Island (21° S, 55° E) for long-term atmospheric remote sensing and in situ measurements. Atmospheric Meas. Tech. 6 (10), 2865–2877. http://dx.doi.org/10.5194/amt-6-2865-2013.

Beig, G., 2011. Long-term trends in the temperature of the mesosphere/lower thermosphere region: 1. Anthropogenic influences. J. Geophys. Res. Atmospheres 116 (A2), n/a. http://dx.doi.org/10.1029/2011ja016646.

Beig, G., Keckhut, P., Lowe, R.P., Roble, R.G., Mlynczak, M.G., Scheer, J., Fomichev, V.I., Offermann, D., French, J., Shepherd, M.G., Semenov, A.I., Remsberg, E.E., She, C.Y., Lübken, F.-J., Bremer, J., Clemesha, B.R., Stegman, J., Sigernes, F., Fadnavis, S., 2003. Review of mesospheric temperature trends. Rev. Geophys. 41 (4), http://dx.doi.org/10.1029/2002rg000121.

Blanc, E., Ceranna, L., Hauchecorne, A., Charlton-Perez, A., Marchetti, E., Evers, L.G., Kvaerna, T., Lastovicka, J., Eliasson, L., Crosby, N.B., Blanc-Benon, P., Pichon, A.L., Brachet, N., Pilger, C., Keckhut, P., Assink, J.D., Smets, P.S.M., Lee, C.F., Kero, J., Sindelarova, T., Kämpfer, N., Rüfenacht, R., Farges, T., Millet, C., Näsholm, S.P., Gibbons, S.J., Espy, P.J., Hibbins, R.E., Heinrich, P., Ripepe, M., Khaykin, S., Mze, N., Chum, J., 2017. Toward an improved representation of middle atmospheric dynamics thanks to the ARISE project. Surv. Geophys. 39 (2), 171–225. http://dx.doi.org/10.1007/s10712-017-9444-0.

Braathen, G.O., Godin-Beekmann, S., Keckhut, P., Mcgee, T.J., Gross, M.R., Vialle, C., Hauchecorne, A., 2004. Intercomparison of stratospheric ozone and temperature measurements at the observatoire de haute provence during the OTOIC NDSC validation campaign from 1–18 july 1997. URL https://hal.science/hal-00327912v1.

Chanin, M.L., Hauchecorne, A., 1984. Lidar studies of temperature and density using Rayleigh scattering. In: International Council of Scientific Unions Middle Atmosphere Handbook. Vol. 13, pp. 87–98, Vol. 13 p. 87-98 (SEE N85-17452 08-46).

Dube, K., Tegtmeier, S., Bourassa, A., Zawada, D., Degenstein, D., Randel, W., Davis, S., Schwartz, M., Livesey, N., Smith, A., 2024. Upper stratospheric temperature trends: New results from OSIRIS. Eur. Geosci. Union http://dx.doi.org/10.5194/egusphere-2024-1252.

Dunkerton, T.J., 1997. The role of gravity waves in the quasi-biennial oscillation. J. Geophys. Res. Atmospheres 102 (D22), 26053–26076. http://dx.doi.org/10.1029/96jd02999.

Emmert, J.T., Drob, D.P., Bernath, P.F., Siskind, D.E., Jones, M., Mlynczak, M.G., Bernath, P.F., Chu, X., Doornbos, E., Funke, B., Гончаренко, Л.П., Hervig, M.E., Schwartz, M., Sheese, P.E., Vargas, F., Williams, B.P., Yuan, T., 2021. NRLMSIS 2.0: A Whole-Atmosphere empirical model of temperature and neutral species densities. Earth Space Sci. 8 (3), http://dx.doi.org/10.1029/2020ea001321.

Fiedler, J., Baumgarten, G., 2024. The ALOMAR Rayleigh/mie/Raman lidar: status after 30 years of operation. Atmospheric Meas. Tech. 17 (19), 5841–5859. http://dx.doi.org/10.5194/amt-17-5841-2024.

Fishbein, E., Cofield, R.E., Froidevaux, L., Jarnot, R.F., Lungu, T.A., Read, W.G., Shippony, Z., Waters, J.W., McDermid, I.S., McGee, T.J., Singh, U.N., Gross, M.R., Hauchecorne, A., Keckhut, P., Gelman, M.E., Nagatani, R.M., 1996. Validation of UARS Microwave Limb Sounder temperature and pressure measurements. J. Geophys. Res. 101 (D6), 9983–10016. http://dx.doi.org/10.1029/95jd03791.

Gerding, M., Kopp, M., Höffner, J., Baumgarten, K., Lübken, F.-J., 2016. Mesospheric temperature soundings with the new, daylight-capable IAP RMR lidar. Atmospheric Meas. Tech. 9 (8), 3707–3715. http://dx.doi.org/10.5194/amt-9-3707-2016.

Gille, J.C., Bailey, P.L., Massie, S.T., Lyjak, L.V., Edwards, D.P., Roche, A.E., Kumer, J.B., Mergenthaler, J.L., Gross, M.R., Hauchecorne, A., Keckhut, P., McGee, T.J., McDermid, I.S., Miller, A.J., Singh, U.N., 1996. Accuracy and precision of cryogenic limb array etalon spectrometer (CLAES) temperature retrievals. J. Geophys. Res. 101 (D6), 9583–9601. http://dx.doi.org/10.1029/96jd00052.

Hampson, J., Keckhut, P., Hauchecorne, A., Chanin, M., 2005. The effect of the 11-year solar-cycle on the temperature in the upper-stratosphere and mesosphere: Part II numerical simulations and the role of planetary waves. J. Atmos. Sol.-Terr. Phys. 67 (11), 948–958. http://dx.doi.org/10.1016/j.jastp.2005.03.005.

Hauchecorne, A., Chanin, M.-L., 1980. Density and temperature profiles obtained by LIDAR between 35 and 70 km. Geophys. Res. Lett. 7 (8), 565–568. http://dx.doi.org/10.1029/gl007i008p00565.

Hauchecorne, A., Chanin, M.-L., Keckhut, P., 1991. Climatology and trends of the middle atmospheric temperature (33–87 km) as seen by Rayleigh lidar over the south of France. J. Geophys. Res. Atmospheres 96 (D8), 15297–15309. http://dx.doi.org/10.1029/91jd01213.

Hersbach, H., Bell, B., Berrisford, P., Hirahara, S., Horányi, Á., Muñoz-Sabater, J., Nicolas, J.P., Peubey, C., Radu, R., Schepers, D., Simmons, A.J., Soci, C., Abdalla, S., Abellan, X., Balsamo, G., Bechtold, P., Biavati, G., Bidlot, J.-R., Bonavita, M., De Chiara, G., Dahlgren, P., Dee, D., Diamantakis, M., Dragani, R., Flemming, J., Forbes, R.M., Fuentes, M., Geer, A., Haimberger, L., Healy, S.B., Hogan, R.J., Hólm, E., Janisková, M., Keeley, S., Laloyaux, P., Lopez, P., Lupu, C., Radnóti, G., De Rosnay, P., Rozum, I., Vamborg, F., Villaume, S., Thépaut, J.-n., 2020. The ERA5 global reanalysis. Q. J. R. Meteorol. Soc. 146 (730), 1999–2049. http://dx.doi.org/10.1002/qj.3803.

Hervig, M.E., Russell, J.M., Gordley, L.L., Park, J.H., Drayson, S.R., Deshler, T., 1996. Validation of aerosol measurements from the halogen occultation experiment. J. Geophys. Res. 101 (D6), 10267–10275. http://dx.doi.org/10.1029/95jd02464.

Holton, J.R., Lindzen, R.S., 1972. An updated theory for the Quasi-Biennial cycle of the tropical stratosphere. J. Atmos. Sci. 29 (6), 1076–1080. http://dx.doi.org/10.1175/1520-0469(1972)029, URL https://doi.org/10.1175/1520-0469(1972)029<1076:autftq>2.0.co;2.

Holton, J.R., Tan, H.-C., 1980. The influence of the equatorial Quasi-Biennial Oscillation on the global circulation at 50 mb. J. Atmos. Sci. 37 (10), 2200–2208. http://dx.doi.org/10.1175/1520-0469(1980)037, URL https://doi.org/10.1175/1520-0469(1980)037<2200:tioteq>2.0.co;2.

Hood, L.L., Jirikowic, J.L., McCormack, J.P., 1993b. Quasi-Decadal variability of the stratosphere: influence of Long-Term Solar Ultraviolet variations. J. Atmos. Sci. 50 (24), 3941–3958. http://dx.doi.org/10.1175/1520-0469(1993)050, URL https://doi.org/10.1175/1520-0469(1993)050<3941:qdvots>2.0.co;2.

Hood, L.L., McPeters, R.D., McCormack, J.P., Flynn, L.E., Hollandsworth, S.M., Gleason, J.F., 1993a. Altitude dependence of stratospheric ozone trends based on Nimbus 7 SBUV data. Geophys. Res. Lett. 20 (23), 2667–2670. http://dx.doi.org/10.1029/93gl03087.

Huang, F.T., Mayr, H.G., Reber, C.A., Russell, J.M., Mengel, J.G., 2006. Stratospheric and mesospheric temperature variations for the quasi-biennial and semiannual (QBO and SAO) oscillations based on measurements from SABER (TIMED) and MLS (UARS). Ann. Geophys. 24 (8), 2131–2149. http://dx.doi.org/10.5194/angeo-24-2131-2006.

Jalali, A., Sica, R.J., Haefele, A., 2018. Improvements to a long-term Rayleigh-scatter lidar temperature climatology by using an optimal estimation method. Atmospheric Meas. Tech. 11 (11), 6043–6058. http://dx.doi.org/10.5194/amt-11-6043-2018.

Kaifler, B., Kaifler, N., 2021. A compact Rayleigh Autonomous Lidar (CORAL) for the middle atmosphere. Atmospheric Meas. Tech. 14 (2), 1715–1732. http://dx.doi.org/10.5194/amt-14-1715-2021.

Keckhut, P., Cagnazzo, C., Chanin, M.-l., Claud, C., Hauchecorne, A., 2005. The 11-year solar-cycle effects on the temperature in the upper-stratosphere and mesosphere: Part I—Assessment of observations. J. Atmos. Sol.-Terr. Phys. 67 (11), 940–947. http://dx.doi.org/10.1016/j.jastp.2005.01.008.

Keckhut, P., Hauchecorne, A., Chanin, M.-L., 1993. A critical review of the database acquired for the long-term surveillance of the middle atmosphere by the french Rayleigh lidars. J. Atmos. Ocean. Technol. 10 (6), 850–867. http://dx.doi.org/10.1175/1520-0426(1993)010, URL https://doi.org/10.1175/1520-0426(1993)010<0850:acrotd>2.0.co;2.

Keckhut, P., Hauchecorne, A., Chanin, M.L., 1995. Midlatitude long-term variability of the middle atmosphere: Trends and cyclic and episodic changes. J. Geophys. Res. Atmospheres 100 (D9), 18887–18897. http://dx.doi.org/10.1029/95jd01387.

Keckhut, P., McDermid, S., Swart, D., McGee, T., Godin-Beekmann, S., Adriani, A., Barnes, J., Baray, J.-L., Bencherif, H., Claude, H., Di Sarra, A.G., Fiocco, G., Hansen, G., Hauchecorne, A., Leblanc, T., Lee, C.H., Pal, S., Megie, G., Nakane, H., Neuber, R., Steinbrecht, W., Thayer, J., 2004. Review of ozone and temperature lidar validations performed within the framework of the Network for the Detection of Stratospheric Change. JEM 6 (9), 721. http://dx.doi.org/10.1039/b404256e.

Keckhut, P., Randel, W., Claud, C., Leblanc, T., Steinbrecht, W., Funatsu, B., Bencherif, H., McDermid, I., Hauchecorne, A., Long, C., Lin, R., Baumgarten, G., 2011. An evaluation of uncertainties in monitoring middle atmosphere temperatures with the ground-based lidar network in support of space observations. J. Atmos. Sol.-Terr. Phys. 73 (5–6), 627–642. http://dx.doi.org/10.1016/j.jastp.2011.01.003.

Kerzenmacher, T.E., Keckhut, P., Hauchecorne, A., Chanin, M.-L., 2006. Methodological uncertainties in multi-regression analyses of middle-atmospheric data series. JEM 8 (7), 682. http://dx.doi.org/10.1039/b603750j.

Khaykin, S., Legras, B., Bucci, S., Sellitto, P., Isaksen, L., Tencé, F., Bekki, S., Bourassa, A., Rieger, L., Zawada, D., Jumelet, J., Godin-Beekmann, S., 2020. The 2019/20 Australian wildfires generated a persistent smoke-charged vortex rising up to 35 km altitude. Commun. Earth Environ. 1 (1), http://dx.doi.org/10.1038/s43247-020-00022-5.

Khaykin, S., Podglajen, A., Ploeger, F., Grooß, J.-U., Tence, F., Bekki, S., Khlopenkov, K., Bedka, K., Rieger, L., Baron, A., Godin-Beekmann, S., Legras, B., Sellitto, P., Sakai, T., Barnes, J., Uchino, O., Morino, I., Nagai, T., Wing, R., Baumgarten, G., Gerding, M., Duflot, V., Payen, G., Jumelet, J., Querel, R., Liley, B., Bourassa, A., Clouser, B., Feofilov, A., Hauchecorne, A., Ravetta, F., 2022. Global perturbation of stratospheric water and aerosol burden by Hunga eruption. Commun. Earth & Environ. 3 (1), http://dx.doi.org/10.1038/s43247-022-00652-x.

Kishore, P., Ratnam, M.V., Velicogna, I., Sivakumar, V., Bencherif, H., Clemesha, B.R., Simonich, D.M., Batista, P.P., Beig, G., 2014. Long-term trends observed in the middle atmosphere temperatures using ground based LIDARs and satellite borne measurements. Ann. Geophys. 32 (3), 301–317. http://dx.doi.org/10.5194/angeo-32-301-2014.

Kozubek, M., Laštovička, J., Zajicek, R., 2021. Climatology and long-term trends in the stratospheric temperature and wind using ERA5. Remote. Sens. 13 (23), 4923. http://dx.doi.org/10.3390/rs13234923.

Kurylo, M.J., Solomon, S., 1990. Network for the Detection of Stratospheric Change. Tech. Rep. NASA Report, Code EEU.

Leblanc, T., McDermid, I.S., Hauchecorne, A., Keckhut, P., 1998a. Evaluation of optimization of lidar temperature analysis algorithms using simulated data. J. Geophys. Res. 103 (D6), 6177–6187. http://dx.doi.org/10.1029/97jd03494.

Leblanc, T., McDermid, I.S., Keckhut, P., Hauchecorne, A., She, C.Y., Krueger, D.A., 1998b. Temperature climatology of the middle atmosphere from long-term lidar measurements at mid- and low-latitudes. J. Geophys. Res..

Li, T., Leblanc, T., McDermid, I.S., Keckhut, P., Hauchecorne, A., Dou, X., 2011. Middle atmosphere temperature trend and solar cycle revealed by long-term Rayleigh lidar observations. J. Geophys. Res. Atmospheres 116, http://dx.doi.org/10.1029/2010jd015275.

Lindzen, R.S., Holton, J.R., 1968. A theory of the Quasi-Biennial oscillation. J. Atmos. Sci. 25 (6), 1095–1107. http://dx.doi.org/10.1175/1520-0469(1968)025, URL https://doi.org/10.1175/1520-0469(1968)025<1095:atotqb>2.0.co;2.

Marchand, M., Keckhut, P., Lefebvre, S., Claud, C., Cugnet, D., Hauchecorne, A., Lefèvre, F., Lefebvre, M.-p., Jumelet, J., Lott, F., Hourdin, F., Thuillier, G., Poulain, V., Bossay, S., Lemennais, P., David, C., Bekki, S., 2011. Dynamical amplification of the stratospheric solar response simulated with the Chemistry-Climate Model LMDz-Reprobus. J. Atmos. Sol.-Terr. Phys. 75–76, 147–160. http://dx.doi.org/10.1016/j.jastp.2011.11.008.

Mariaccia, A., Keckhut, P., Hauchecorne, A., Claud, C., Pichon, A.L., Meftah, M., Khaykin, S., 2022. Assessment of ERA-5 temperature variability in the middle atmosphere using Rayleigh LIDAR measurements between 2005 and 2020. Atmosphere 13 (2), 242. http://dx.doi.org/10.3390/atmos13020242.

Marlton, G., Charlton-Perez, A., Harrison, G., Polichtchouk, I., Hauchecorne, A., Keckhut, P., Wing, R., Leblanc, T., Steinbrecht, W., 2021. Using a network of temperature LIDARs to identify temperature biases in the upper stratosphere in ECMWF reanalyses. Atmospheric Chem. Phys. 21 (8), 6079–6092. http://dx.doi.org/10.5194/acp-21-6079-2021.

Martin, Z., Sobel, A., Butler, A., Wang, S., 2020. Variability in QBO Temperature anomalies on annual and decadal time scales. J. Clim. 34 (2), 589–605. http://dx.doi.org/10.1175/jcli-d-20-0287.1.

McGee, T.J., Whiteman, D.N., Ferrare, R.A., Butler, J.J., Burris, J.F., 1991. STROZ LITE: Stratospheric ozone lidar trailer experiment. Opt. Eng., Bellingham 30 (1), 31. http://dx.doi.org/10.1117/12.55771.

Organization, W.M., Programme, U.N.E., Oceanic, N., Administration, A., Aeronautics, N., Administration, S., Commission, E., 2018. WMO (World Meteorological Organization), Scientific Assessment of Ozone Depletion: 2018. Global Ozone Research and Monitoring Project–Report No. 58, p. 588, URL http://ozone.unep.org/science/assessment/sap.

Peterson, D.A., Campbell, J.R., Hyer, E.J., Fromm, M.D., Kablick, G.P., Cossuth, J.H., DeLand, M.T., 2018. Wildfire-driven thunderstorms cause a volcano-like stratospheric injection of smoke. Npj Clim. Atmospheric Sci. 1 (1), http://dx.doi.org/10.1038/s41612-018-0039-3.

Polichtchouk, I., Van Niekerk, A., Wedi, N., 2022. Resolved gravity waves in the extratropical stratosphere: Effect of horizontal resolution increase from O(10) to O(1) km. J. Atmos. Sci. 80 (2), 473–486. http://dx.doi.org/10.1175/jas-d-22-0138.1.

Salawitch, R.J., Smith, J.B., Selkirk, H., Wargan, K., Chipperfield, M.P., Hossaini, R., Levelt, P.F., Livesey, N.J., McBride, L.A., Millán, L.F., Moyer, E., Santee, M.L., Schoeberl, M.R., Solomon, S., Stone, K., Worden, H.M., 2025. The Imminent data Desert: The future of stratospheric monitoring in a rapidly changing world. Bull. Am. Meteorol. Soc. http://dx.doi.org/10.1175/bams-d-23-0281.1.

Sica, R.J., Haefele, A., 2015. Retrieval of temperature from a multiple-channel Rayleigh-scatter lidar using an optimal estimation method. Appl. Opt. 54 (8), 1872. http://dx.doi.org/10.1364/ao.54.001872.

Sica, R.J., Sargoytchev, S., Argall, P.S., Borra, E.F., Girard, L., Sparrow, C.T., Flatt, S., 1995. Lidar measurements taken with a large-aperture liquid mirror 1 Rayleigh-scatter system. Appl. Opt. 34 (30), 6925. http://dx.doi.org/10.1364/ao.34.006925.

Singh, U.N., Keckhut, P., McGee, T.J., Gross, M.R., Hauchecorne, A., Fishbein, E., Waters, J.W., Gille, J.C., Roche, A.E., Russell, J.M., 1996. Stratospheric temperature measurements by two collocated NDSC lidars during UARS validation campaign. J. Geophys. Res. 101 (D6), 10287–10297. http://dx.doi.org/10.1029/96jd00516.

Sofieva, V.F., Rozanov, A., Szelag, M., Burrows, J.P., Retscher, C., Damadeo, R., Degenstein, D., Rieger, L.A., Bourassa, A., 2024. CREST: a climate data record of stratospheric aerosols. Earth Syst. Sci. Data 16 (11), 5227–5241. http://dx.doi.org/10.5194/essd-16-5227-2024.

Steinbrecht, W., Claude, H., Schönenborn, F., McDermid, I.S., Leblanc, T., Godin-Beekmann, S., Keckhut, P., Hauchecorne, A., Van Gijsel, J.A.E., Swart, D.P.J., Bodeker, G.E., Parrish, A., Boyd, I.S., Kämpfer, N., Hocke, K., Stolarski, R.S., Frith, S.M., Thomason, L.W., Remsberg, E.E., Von Savigny, C., Rozanov, A., Burrows, J.P., 2009. Ozone and temperature trends in the upper stratosphere at five stations of the Network for the Detection of Atmospheric Composition Change. Int. J. Remote Sens. 30 (15–16), 3875–3886. http://dx.doi.org/10.1080/01431160902821841.

Steinbrecht, W., Velazco, V.A., Dirksen, R., Doppler, L., Oelsner, P., Van Malderen, R., De Backer, H., Barras, E.M., Stübi, R., Godin-Beekmann, S., Hauchecorne, A., 2025. Ground-based monitoring of stratospheric ozone and temperature over Germany since the 1960s. Earth Space Sci. 12 (3), http://dx.doi.org/10.1029/2024ea003821.

Steiner, A.K., Ladstädter, F., Randel, W.J., Maycock, A.C., Fu, Q., Claud, C., Gleisner, H., Haimberger, L., Ho, S.-p., Keckhut, P., Leblanc, T., Mears, C., Polvani, L.M., Santer, B.D., Schmidt, T., Sofieva, V., Wing, R., Zou, C.-z., 2020. Observed temperature changes in the troposphere and stratosphere from 1979 to 2018. J. Clim. 33 (19), 8165–8194. http://dx.doi.org/10.1175/jcli-d-19-0998.1.

Tufel, N.G., Keckhut, P., Dumas, L., Mariaccia, A., Meftah, M., Courcoux, Y., Vicomte, M., Hauchecorne, A., 2025. Assessment of middle atmosphere climatology using lidar for aerospace applications. Adv. Space Res. http://dx.doi.org/10.1016/j.asr.2025.06.004.

Von Zahn, U., Von Cossart, G., Fiedler, J., Fricke, K.H., Nelke, G., Baumgarten, G., Rees, D., Hauchecorne, A., Adolfsen, K., 2000. The ALOMAR Rayleigh/mie/Raman lidar: objectives, configuration, and performance. Ann. Geophys. 18 (7), 815–833. http://dx.doi.org/10.1007/s00585-000-0815-2.

Wing, R., Godin-Beekmann, S., Steinbrecht, W., McGee, T.J., Sullivan, J.T., Khaykin, S., Sumnicht, G., Twigg, L., 2021. Evaluation of the new DWD ozone and temperature lidar during the hohenpeißenberg Ozone Profiling Study (HOPS) and comparison of results with previous NDACC campaigns. Atmospheric Meas. Tech. 14 (5), 3773–3794. http://dx.doi.org/10.5194/amt-14-3773-2021.

Wing, R., Hauchecorne, A., Keckhut, P., Godin-Beekmann, S., Khaykin, S., McCullough, E.M., Mariscal, J.-F., d'Almeida, É., 2018. Lidar temperature series in the middle atmosphere as a reference data set – Part 1: Improved retrievals and a 20-year cross-validation of two co-located French lidars. Atmospheric Meas. Tech. 11 (10), 5531–5547. http://dx.doi.org/10.5194/amt-11-5531-2018.

Wing, R., Steinbrecht, W., Godin-Beekmann, S., McGee, T.J., Sullivan, J.T., Sumnicht, G., Ancellet, G., Hauchecorne, A., Khaykin, S., Keckhut, P., 2020. Intercomparison and evaluation of ground- and satellite-based stratospheric ozone and temperature profiles above observatoire de haute-provence during the lidar validation NDACC experiment (LAVANDE). Atmospheric Meas. Tech. 13 (10), 5621–5642. http://dx.doi.org/10.5194/amt-13-5621-2020.

(WMO), W.M.O., Oceanic, N., (NOAA), A.A., (UNEP), U.N.E.P., Aeronautics, N., (NASA), S.A., Commission, E., 2023. Scientific Assessment of Ozone Depletion: 2022. Tech. Rep. 978-9914-733-97-6, URL https://library.wmo.int/records/item/58360-scientific-assessment-of-ozone-depletion-2022.

Yamazaki, K., Nakamura, T., Ukita, J., Hoshi, K., 2020. A tropospheric pathway of the stratospheric quasi-biennial oscillation (QBO) impact on the boreal winter polar vortex. Atmospheric Chem. Phys. 20 (8), 5111–5127. http://dx.doi.org/10.5194/acp-20-5111-2020.

Zhao, X.R., Sheng, Z., Shi, H.Q., Weng, L.B., He, Y., 2021. Middle atmosphere temperature changes derived from SABER observations during 2002–2020. J. Clim. 1. http://dx.doi.org/10.1175/jcli-d-20-1010.1.